PHASE DIAGRAMS and MACROMOLECULAR STABILITY

C Russell Middaugh PhD
University of Kansas
Macromolecule and Vaccine Stabilization Laboratory

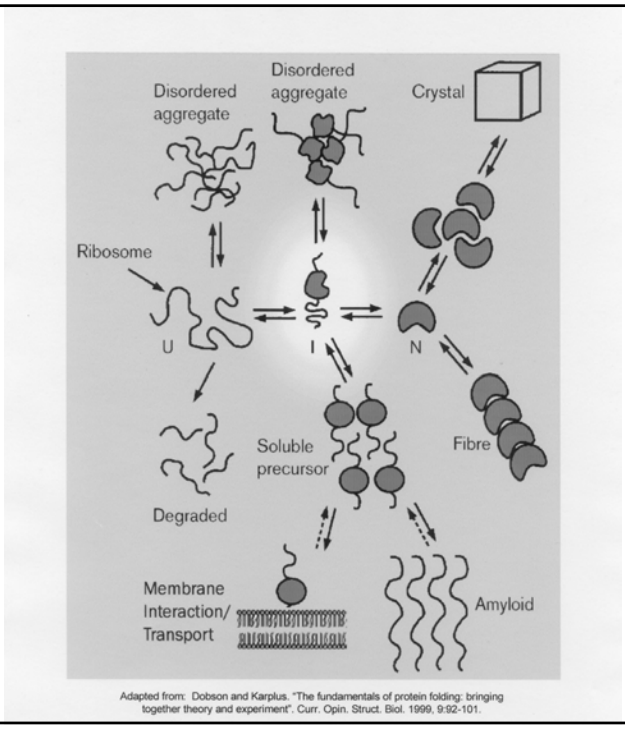

Adapted from: Dobson and Karplus. "The fundamentals of protein folding: bringing together theory and experiment". Curr. Opin. Struct. Biol. 1999, 9:92-101.

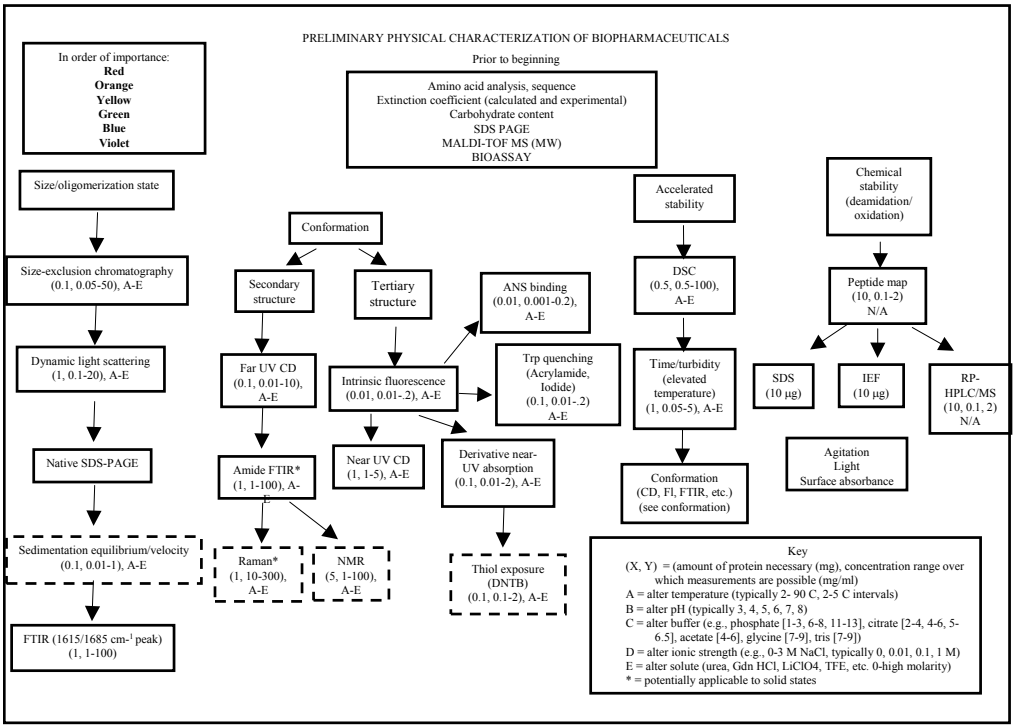
PRELIMINARY PHYSICAL CHARACTERIZATION OF BIOPHARMACEUTICALS
In order of importance:
Red
Orange
Yellow
Green
Blue
Violet
Prior to beginning
Amino acid analysis, sequence
Extinction coefficient (calculated and experimental)
Carbohydrate content
SDS PAGE
MALDI-TOF MS (MW)
BIOASSAY
Size/oligomerization state
Size-exclusion chromatography (0.1, 0.05-50), A-E
Dynamic light scattering (1, 0.1-20), A-E
Native SDS-PAGE
Sedimentation equilibrium/velocity (0.1, 0.01-1), A-E
FTIR (1615/1685 cm-1 peak) (1, 1-100)
Conformation
Secondary structure
Tertiary structure
Far UV CD (0.1, 0.01-10), A-E
Amide FTIR* (1, 1-100), A-E
Raman* (1, 10-300), A-E
NMR (5, 1-100), A-E
Intrinsic fluorescence (0.01, 0.01-.2), A-E
ANS binding (0.01, 0.001-0.2), A-E
Trp quenching (Acrylamide, Iodide) (0.1, 0.01-.2) A-E
Near UV CD (1, 1-5), A-E
Derivative near-UV absorption (0.1, 0.01-2), A-E
Thiol exposure (DNTB) (0.1, 0.1-2), A-E
Accelerated stability
DSC (0.5, 0.5-100), A-E
Time/turbidity (elevated temperature) (1, 0.05-5), A-E
Conformation (CD, Fl, FTIR, etc.) (see conformation)
Chemical stability (deamidation/ oxidation)
Peptide map (10, 0.1-2) N/A
SDS (10 µg)
IEF (10 µg)
RP-HPLC/MS (10, 0.1, 2) N/A
Agitation
Light
Surface absorbance
Key
(X, Y) = (amount of protein necessary (mg), concentration range over which measurements are possible (mg/ml)
A = alter temperature (typically 2- 90 C, 2-5 C intervals)
B = alter pH (typically 3, 4, 5, 6, 7, 8)
C = alter buffer (e.g., phosphate [1-3, 6-8, 11-13], citrate [2-4, 4-6, 5-6.5], acetate [4-6], glycine [7-9], tris [7-9])
D = alter ionic strength (e.g., 0-3 M NaCl, typically 0, 0.01, 0.1, 1 M)
E = alter solute (urea, Gdn HCl, LiClO4, TFE, etc. 0-high molarity)
* = potentially applicable to solid states

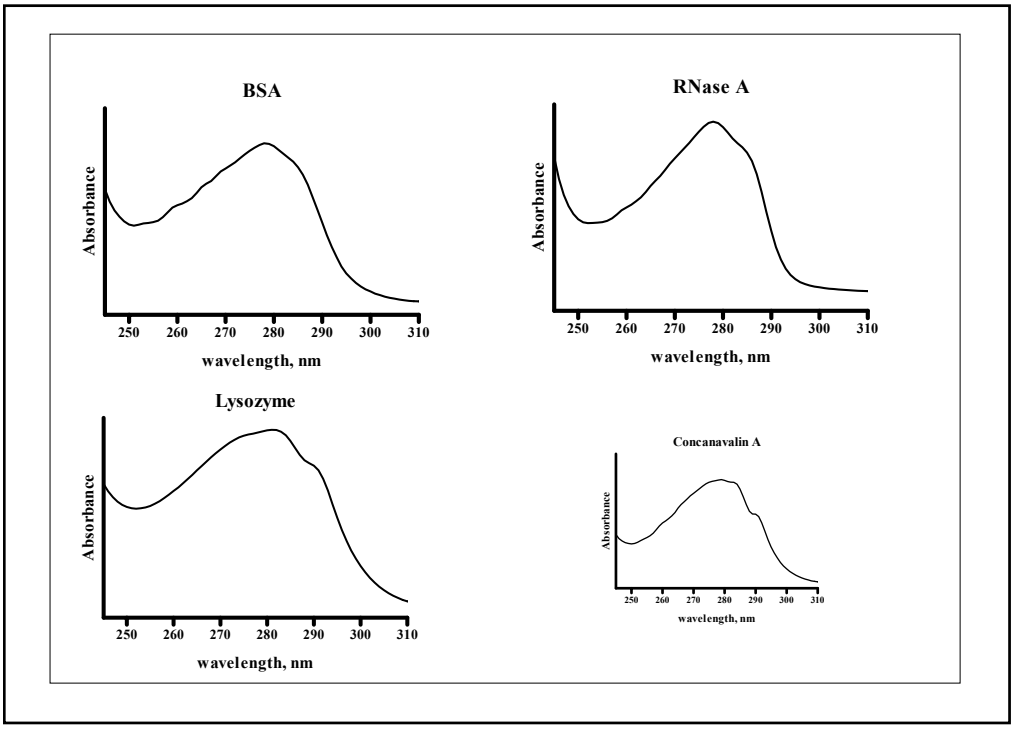
BSA
Absorbance
250 260 270 280 290 300 310
wavelength, nm
RNase A
Absorbance
250 260 270 280 290 300 310
wavelength, nm
Lysozyme
Absorbance
250 260 270 280 290 300 310
wavelength, nm
Concanavalin A
Absorbance
250 260 270 280 290 300 310
wavelength, nm

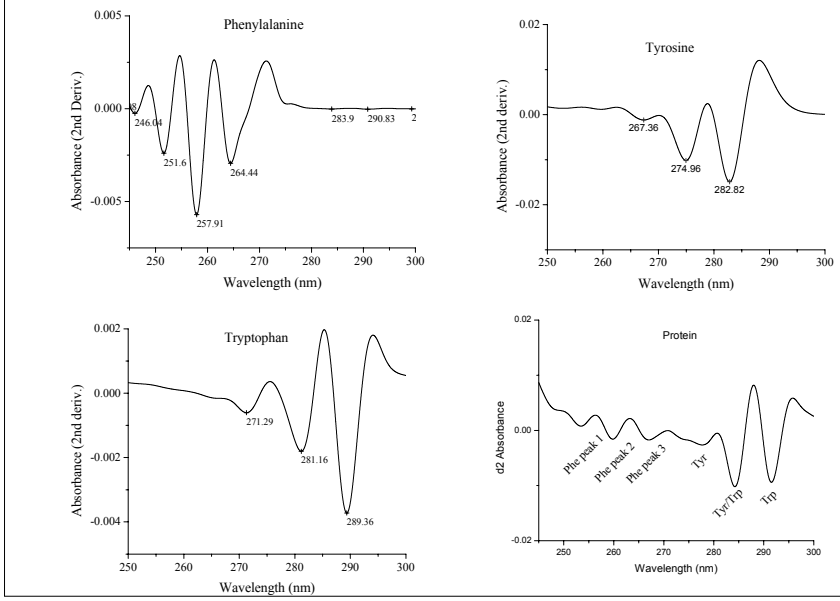

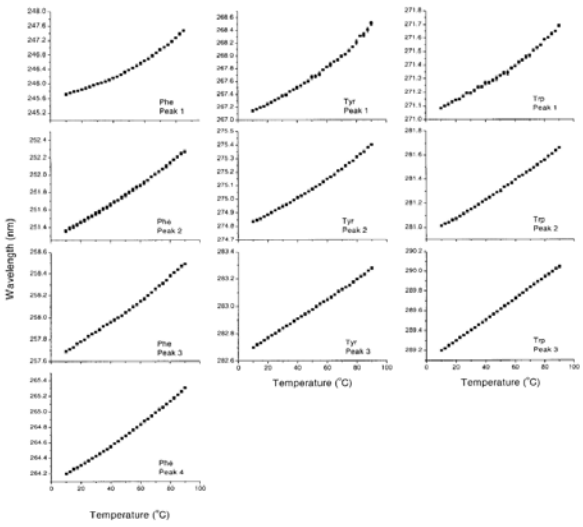

Figure 7. Temperature dependence of absorbance derivative peaks of model amino acids. Spectra were collected at 2.5°C intervals after a 3-min equilibration at temperatures between 10° and 90°C. Model compounds used were: *N*-Ac-L-Trp-OEt (37 μM), *N*-Ac-L-Tyr-OEt (146 μM), and *N*-Ac-L-Phe-OEt (510 μM). All errors are reported as standard error ($n = 3$).

Kueltzo, L.A., Ersoy, B., Ralston, J.P., and Middaugh, C.R. *J. Pharm. Sci.* (2003) **92**, 1805-1820.

Empirical phase diagrams

- Multiple analytical techniques employed to characterize the physical properties of protein therapeutics under various solution conditions (experimental parameters, i.e. pH and temperature)
- A multidimensional phase space approach used to describe patterns connecting resultant complex data sets
- Empirical phases identified to represent parameter regions with substantially uniform and coherent structural data
- A phase diagram constructed employing an RGB color system to allow visualization and interpretation of the complex data sets

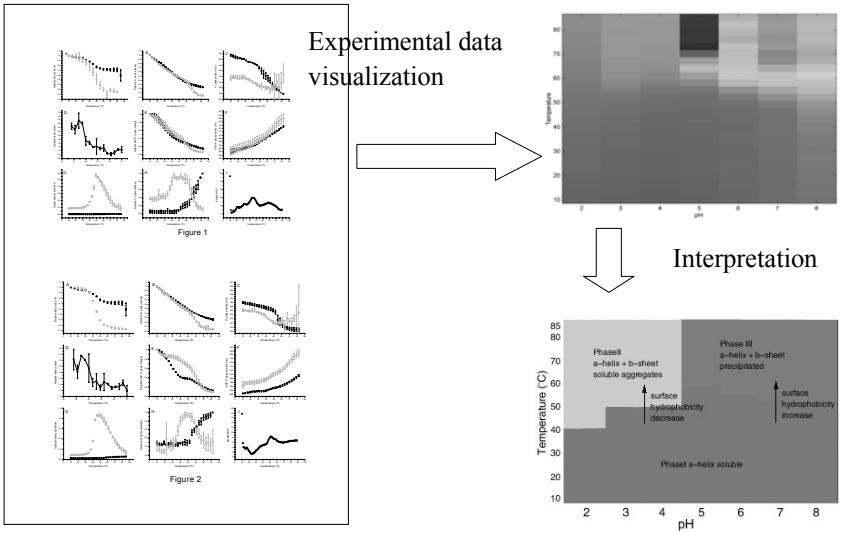

Mathematical process

Construct vector description for all the experimental data at each coordinate (each discrete parameter combination)

Construct density matrix including all the vectors and calculate the eigenvalues and eigenvectors

Re-describe all the experimental data under a new basis set, which is constructed by eigenvectors

According to the magnitude of eigenvalues, truncate the re-descriptions to smaller-dimensioned vectors for visualization

Construct vector descriptions

A set of variables (experimental data) associated with each coordinate was used to construct the vector

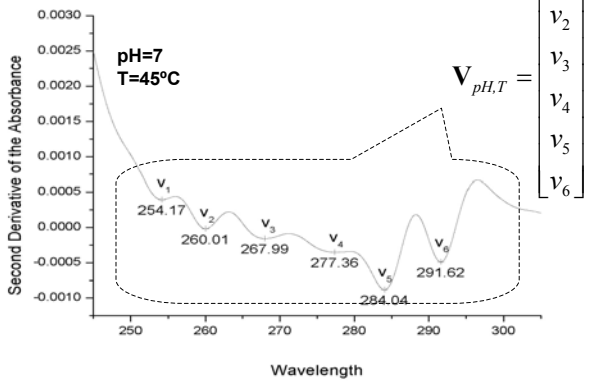

Visualization

Reconstructed 3-D Vector $v^{i}_{pH,T} = (x_1 \quad x_2 \quad x_3)$

Rescale the vector to RGB color system

$$v^{i}_{pH,T}{}' = (x_1' \quad x_2' \quad x_3') \qquad 0 \le x_i^{'} \le 1$$

Each vector will define a color block in the phase diagram at its corresponding coordinates (pH, T)

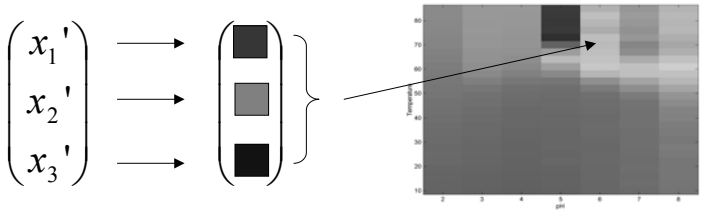

Bovine Granulocyte Colony Stimulating Factor (bGCSF)

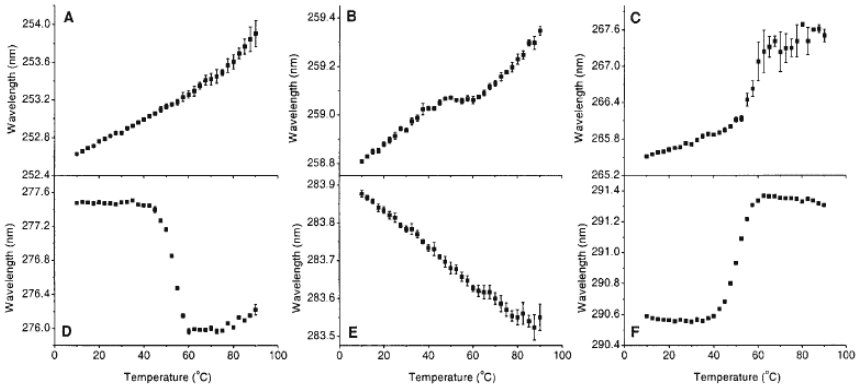

Figure 1. Derivative absorbance studies of bGCSF as a function of temperature at pH 2. The wavelength positions of six negative peaks were followed as a function of temperature: 1(A), Phe; 2(B), Phe; 3(C), Phe; 4(D), Tyr; 5(E), Tyr/Trp; and 6(F), Trp. Protein concentration was 5 μM in 10 mM citrate buffer. Spectra were collected at 2.5°C intervals, with a 5-min temperature equilibration period included before data collection. All errors are reported as standard error ($n = 3$). Error bars that are not visible are hidden within the symbol.

Kueltzo, L.A., Ersoy, B., Ralston, J.P., and Middaugh, C.R. *J. Pharm. Sci.* (2003) **92**, 1805-1820.

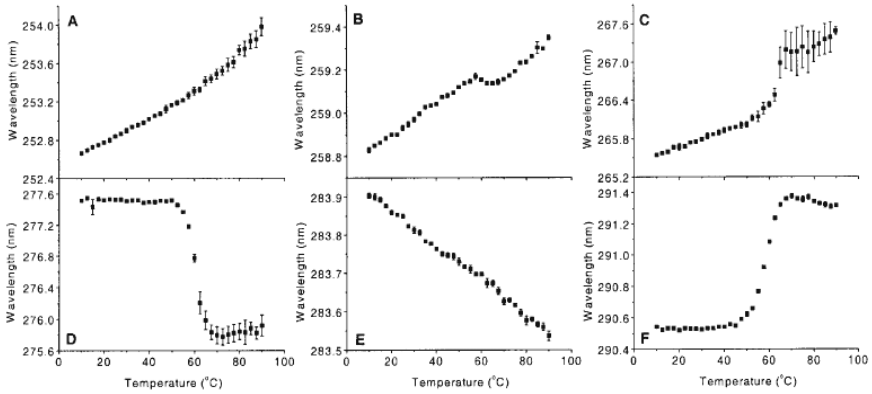

Figure 2. Derivative absorbance studies of bGCSF as a function of temperature at pH 3. The wavelength positions of six negative peaks were followed as a function of temperature: 1(A), Phe; 2(B), Phe; 3(C), Phe; 4(D), Tyr; 5(E), Tyr/Trp; and 6(F), Trp. Protein concentration was 5 μM in 10 mM citrate buffer. Spectra were collected at 2.5°C intervals, with a 5-min temperature equilibration period included before data collection. All errors are reported as standard error ($n = 3$).

Kueltzo, L.A., Ersoy, B., Ralston, J.P., and Middaugh, C.R. *J. Pharm. Sci.* (2003) **92**, 1805-1820.

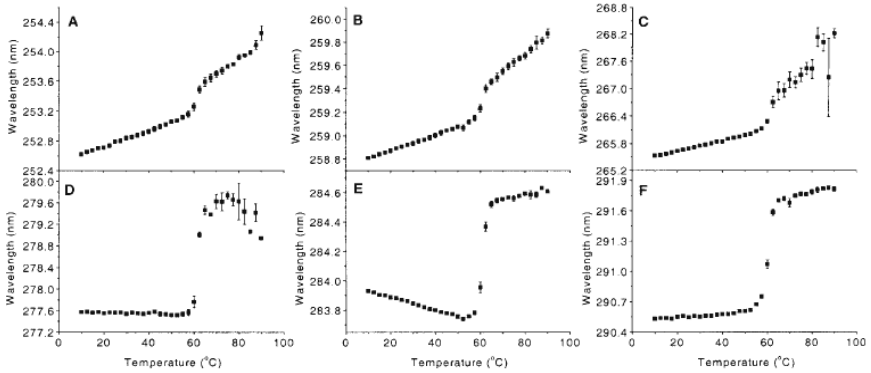

Figure 3. Derivative absorbance studies of bGCSF as a function of temperature at pH 4. The wavelength positions of six negative peaks were followed as a function of temperature: 1(A), Phe; 2(B), Phe; 3(C), Phe; 4(D), Tyr; 5(E), Tyr/Trp; and 6(F), Trp. Protein concentration was 5 μM in 10 mM citrate buffer. Spectra were collected at 2.5°C intervals, with a 5-min temperature equilibration period included before data collection. All errors are reported as standard error ($n = 3$).

Kueltzo, L.A., Ersoy, B., Ralston, J.P., and Middaugh, C.R. *J. Pharm. Sci.* (2003) **92**, 1805-1820.

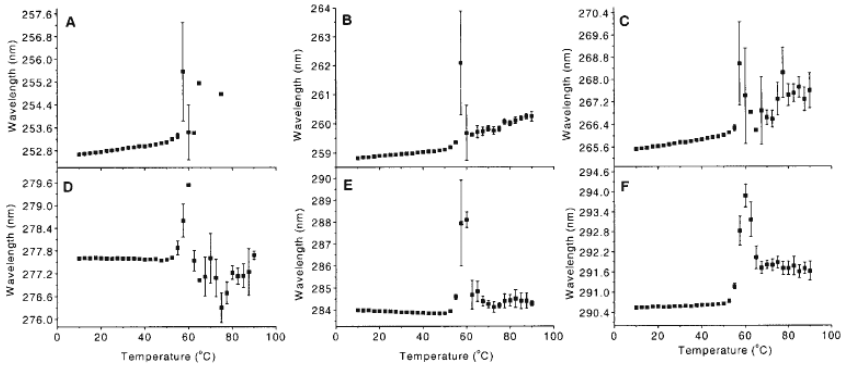

Figure 4. Derivative absorbance studies of bGCSF as a function of temperature at pH 5. The wavelength positions of six negative peaks were followed as a function of temperature: 1(A), Phe; 2(B), Phe; 3(C), Phe; 4(D), Tyr; 5(E), Tyr/Trp; and 6(F), Trp. Protein concentration was 5 μM in 10 mM citrate buffer. Spectra were collected at 2.5°C intervals, with a 5-min temperature equilibration period included before data collection. All errors are reported as standard error ($n = 3$).

Kueltzo, L.A., Ersoy, B., Ralston, J.P., and Middaugh, C.R. *J. Pharm. Sci.* (2003) **92**, 1805-1820.

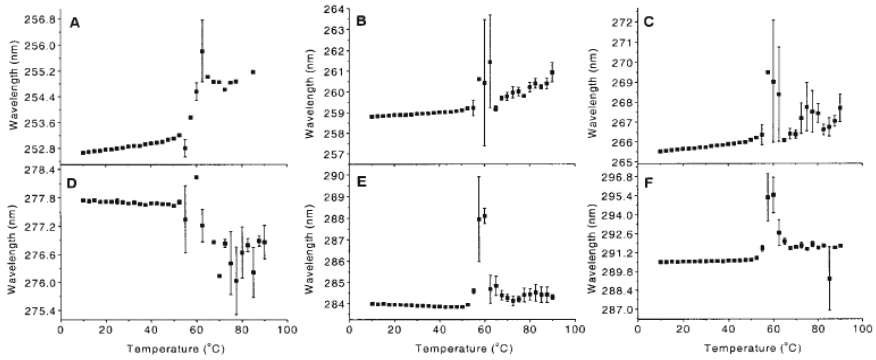

Figure 5. Derivative absorbance studies of bGCSF as a function of temperature at pH 6. The wavelength positions of six negative peaks were followed as a function of temperature: 1(A), Phe; 2(B), Phe; 3(C), Phe; 4(D), Tyr; 5(E), Tyr/Trp; and 6(F), Trp. Protein concentration was 5 μM in 10 mM citrate buffer. Spectra were collected at 2.5°C intervals, with a 5-min temperature equilibration period included before data collection. All errors are reported as standard error ($n = 3$).

Kueltzo, L.A., Ersoy, B., Ralston, J.P., and Middaugh, C.R. *J. Pharm. Sci.* (2003) **92**, 1805-1820.

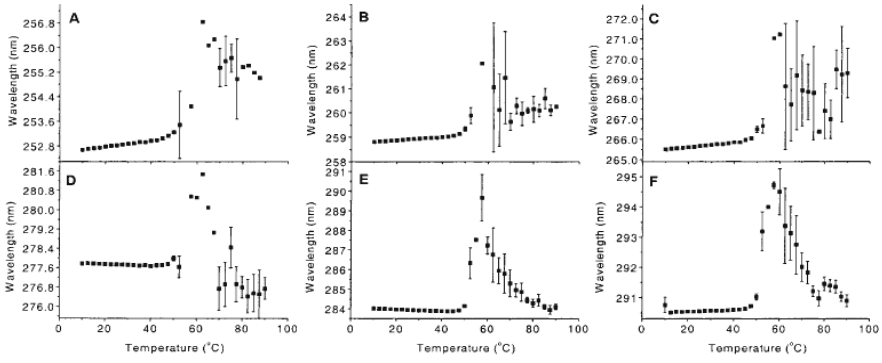

Figure 6. Derivative absorbance studies of bGCSF as a function of temperature at pH 7. The wavelength positions of six negative peaks were followed as a function of temperature: 1(A), Phe; 2(B), Phe; 3(C), Phe; 4(D), Tyr; 5(E), Tyr/Trp; and 6(F), Trp. Protein concentration was 5 μM in 10 mM citrate buffer. Spectra were collected at 2.5°C intervals, with a 5-min temperature equilibration period included before data collection. All errors are reported as standard error ($n = 3$).

Kueltzo, L.A., Ersoy, B., Ralston, J.P., and Middaugh, C.R. *J. Pharm. Sci.* (2003) **92**, 1805-1820.

Table 1. High-Resolution Derivative Absorbance Analysis of bGCSF

Method	pH	Initial λ^a (nm)	Transition Start[b] (°C)	Transition Finish[b] (°C)	Transition Midpoint[c] (°C)	Final λ^a (nm)
Absorbance peak 1	2	252.65 (0.01)	67.5	>90	NA[d]	253.91 (0.14)
	3	252.66 (0.01)	62.0	>90	NA	253.98 (0.09)
	4	252.62 (0.02)	57.5	65.0	61.7 (0.4)	254.26 (0.10)
	5	252.67 (0.01)	50.0	ND (A)[e]	ND (A)	ND (A)
	6	252.67 (0.02)	50.0	65.0	58.5 (1.2)	~255.0
	7	252.68 (0.00)	45.0	65.0	58.5 (1.1)	ND (A)
Absorbance peak 2	2	258.81 (0.01)	47.5	60.0	NA	259.35 (0.02)
	3	258.83 (0.01)	57.5	67.5	NA	259.35 (0.01)
	4	258.81 (0.01)	55.0	65.0	60.8 (0.7)	259.88 (0.04)
	5	258.82 (0.01)	50.0	65.0	ND (A)	260.24 (0.16)
	6	258.82 (0.01)	47.5	65.0	ND (A)	260.93 (0.47)
	7	258.81 (0.01)	47.5	70.0	ND (A)	ND (A)
Absorbance peak 3	2	265.52 (0.00)	47.5	65.0	57.1 (0.4)	265.88 (0.03)
	3	265.55 (0.01)	57.5	67.5	63.7 (0.2)	267.49 (0.06)
	4	265.53 (0.01)	55.0	67.5	61.1 (0.1)	268.22 (0.10)
	5	265.53 (0.01)	52.5	ND (A)	ND (A)	267.59 (0.63)
	6	265.52 (0.01)	50.0	ND (A)	ND (A)	267.70 (0.70)
	7	265.50 (0.01)	45.0	ND (A)	ND (A)	269.28 (1.24)
Absorbance peak 4	2	277.48 (0.02)	40.0	62.5	53.4 (0.2)	276.22 (0.06)
	3	277.52 (0.01)	52.5	72.5	60.5 (0.1)	275.92 (0.14)
	4	277.58 (0.01)	57.5	72.5	61.6 (0.2)	ND (A)
	5	277.60 (0.01)	52.5	ND (A)	ND (A)	277.68 (0.11)
	6	277.74 (0.01)	55.0	ND (A)	ND (A)	276.86 (0.35)
	7	277.77 (0.02)	47.5	ND (A)	ND (A)	276.74 (0.44)
Absorbance peak 5	2	283.88 (0.01)	82.5	>90	NA	283.75 (0.01)
	3	283.90 (0.01)	NA	NA	NA	283.54 (0.01)
	4	283.93 (0.00)	55.0	67.5	61.2 (0.0)	284.61 (0.01)
	5	283.95 (0.01)	52.5	67.5	60.0	284.38 (0.13)
	6	283.99 (0.01)	50.0	67.5	60.0	284.29 (0.11)
	7	284.02 (0.01)	47.5	NA	57.5	284.10 (0.14)
Absorbance peak 6	2	290.59 (0.01)	37.5	67.5	50.6 (0.1)	290.58 (0.01)
	3	290.54 (0.00)	37.5	70.0	59.3 (0.1)	291.32 (0.01)
	4	290.53 (0.01)	52.5	65.0	60.4 (0.1)	291.81 (0.02)
	5	290.54 (0.00)	52.5	67.5	60.0	291.62 (0.28)
	6	290.51 (0.01)	52.5	67.5	60.0	291.69 (0.07)
	7	290.76 (0.25)	45.0	NA	57.5	290.90 (0.20)

[a]Standard error calculated from $n = 3$.
[b]Transition range was defined as temperatures where values deviated from initial or terminal slope.
[c]Midpoints determined by fit to sigmoidal function, where error values are error of fit, or defined as the peak of the transition for non-sigmoidal plots.
[d]NA: parameter is not applicable to the observed data.
[e]ND (A): parameter could not be determined as a result of excess noise in the data caused by aggregated samples.

Kueltzo, L.A., Ersoy, B., Ralston, J.P., and Middaugh, C.R. *J. Pharm. Sci.* (2003) **92**, 1805-1820.

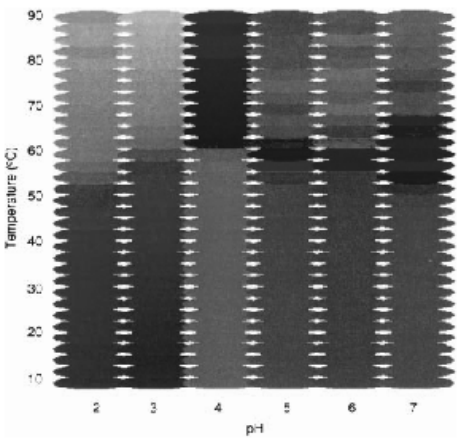

Figure 9. Temperature–pH phase diagram of bGCSF based on second-derivative absorbance data. Six distinct phases are observed: (1) pH 2–3, T 10°–55°C; (2) pH 2–3, T 55°–90°C; (3) pH 4, T 10°–60°C; (4) pH 4, T 60°–90°C; (5) pH 5–7, T 10°–50°C; and (6) pH 5–7, T 50°–90°C. Blocks of continuous color represent single phases, conditions under which the raw data-derived vectors behave similarly. The colors were arbitrarily chosen.

Kueltzo, L.A., Ersoy, B., Ralston, J.P., and Middaugh, C.R. *J. Pharm. Sci.* (2003) **92**, 1805-1820.

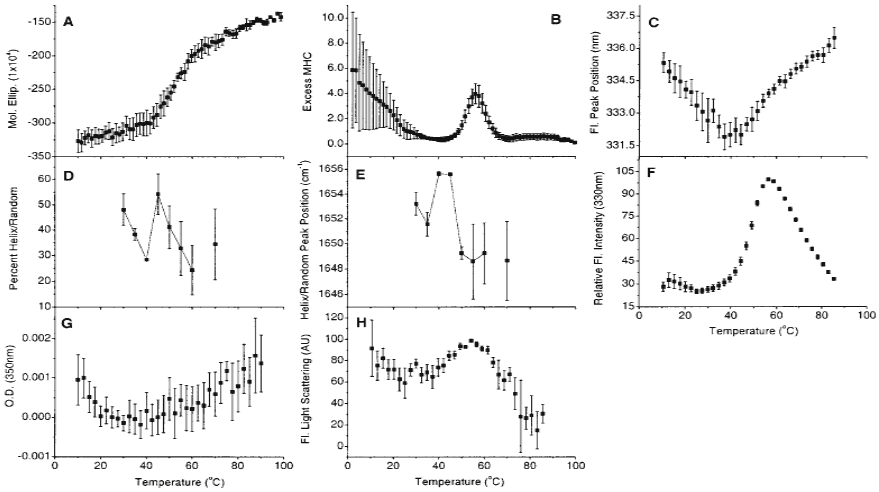

Figure 1. Characterization of bGCSF as a function of temperature at pH 2. (A) CD: ellipticity at 208 nm. (B) DSC: excess molar heat capacity. (C) Fluorescence: tryptophan peak wavelength shift. (D) FTIR: helix/random percentage. (E) FTIR: helix/random peak position. (F) Fluorescence: tryptophan emission intensity at 330 nm. (G) Temperature-induced aggregation: OD at 350 nm. (H) Rayleigh scattering during fluorescence. All errors are reported as standard error ($n = 3$).

Kueltzo L.A. and Middaugh, C.R. *J. Pharm. Sci*. (2003) **92,** 1793-1804.

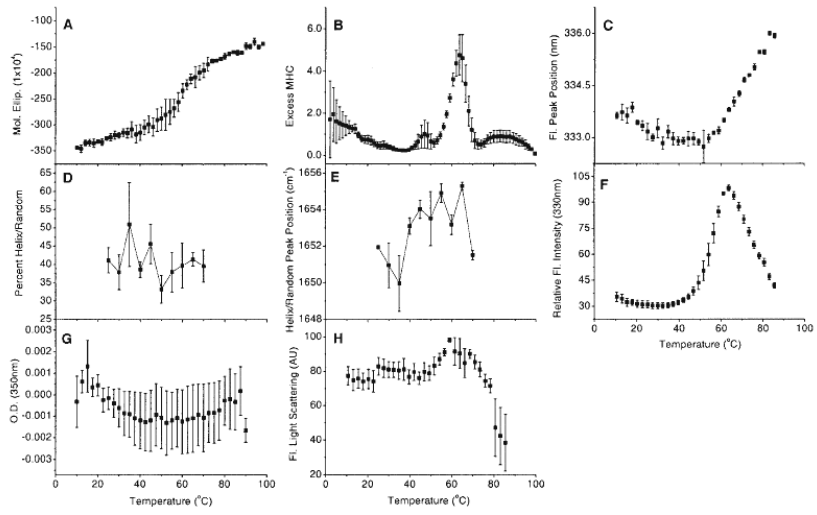

Figure 2. Characterization of bGCSF as a function of temperature at pH 3. (A) CD: ellipticity at 208 nm. (B) DSC: excess molar heat capacity. (C) Fluorescence: tryptophan peak wavelength shift. (D) FTIR: helix/random percentage. (E) FTIR: helix/random peak position. (F) Fluorescence: tryptophan emission intensity at 330 nm. (G) Temperature-induced aggregation: OD at 350 nm. (H) Rayleigh scattering during fluorescence. All errors are reported as standard error ($n = 3$).

Kueltzo L.A. and Middaugh, C.R. *J. Pharm. Sci*. (2003) **92,** 1793-1804.

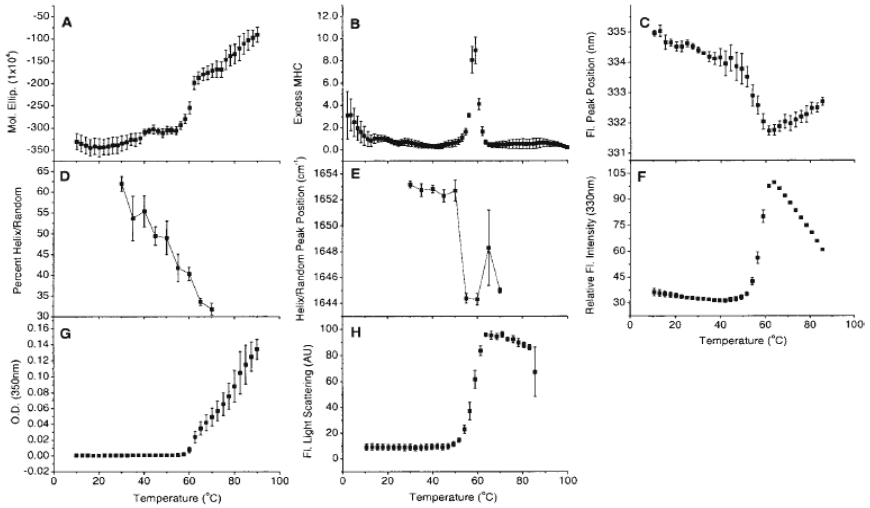

Figure 3. Characterization of bGCSF as a function of temperature at pH 4. (A) CD: ellipticity at 208 nm. (B) DSC: excess molar heat capacity. (C) Fluorescence: tryptophan peak wavelength shift. (D) FTIR: helix/random percentage. (E) FTIR: helix/random peak position. (F) Fluorescence: tryptophan emission intensity at 330 nm. (G) Temperature-induced aggregation: OD at 350 nm. (H) Rayleigh scattering during fluorescence. All errors are reported as standard error ($n = 3$).

Kueltzo L.A. and Middaugh, C.R. *J. Pharm. Sci*. (2003) **92** 1793-1804.

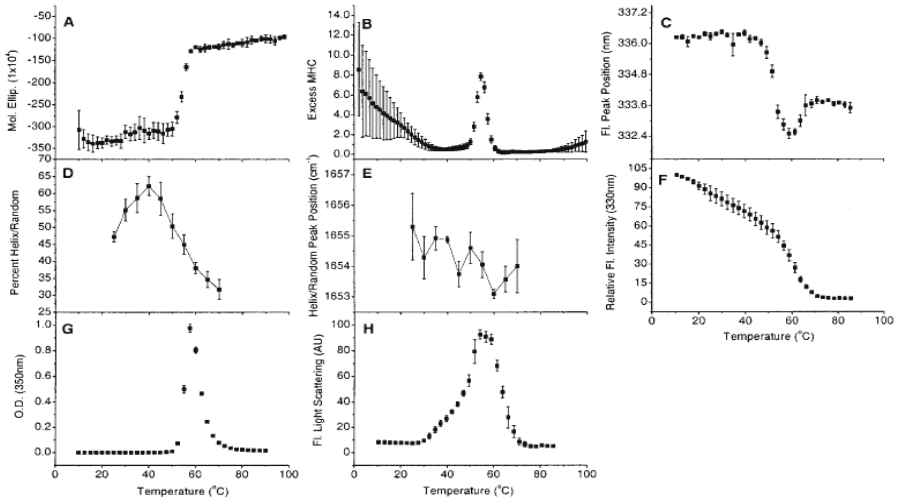

Figure 4. Characterization of bGCSF as a function of temperature at pH 5. (A) CD: ellipticity at 208 nm. (B) DSC: excess molar heat capacity. (C) Fluorescence: tryptophan peak wavelength shift. (D) FTIR: helix/random percentage. (E) FTIR: helix/random peak position. (F) Fluorescence: tryptophan emission intensity at 330 nm. (G) Temperature-induced aggregation: OD at 350 nm. (H) Rayleigh scattering during fluorescence. All errors are reported as standard error ($n = 3$).

Kueltzo L.A. and Middaugh, C.R. *J. Pharm. Sci*. (2003) **92,** 1793-1804.

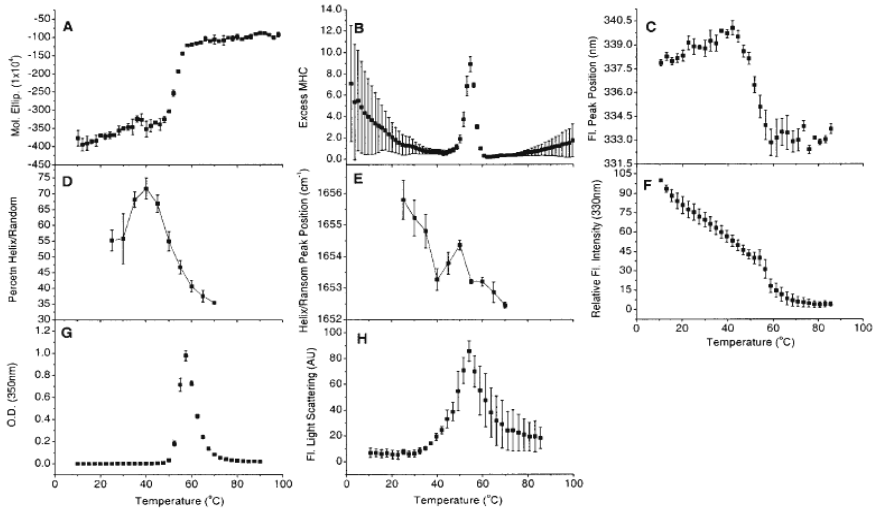

Figure 5. Characterization of bGCSF as a function of temperature at pH 6. (A) CD: ellipticity at 208 nm. (B) DSC: excess molar heat capacity. (C) Fluorescence: tryptophan peak wavelength shift. (D) FTIR: helix/random percentage. (E) FTIR: helix/random peak position. (F) Fluorescence: tryptophan emission intensity at 330 nm. (G) Temperature-induced aggregation: OD at 350 nm. (H) Rayleigh scattering during fluorescence. All errors are reported as standard error ($n = 3$).

Kueltzo L.A. and Middaugh, C.R. *J. Pharm. Sci*. (2003) **92,** 1793-1804.

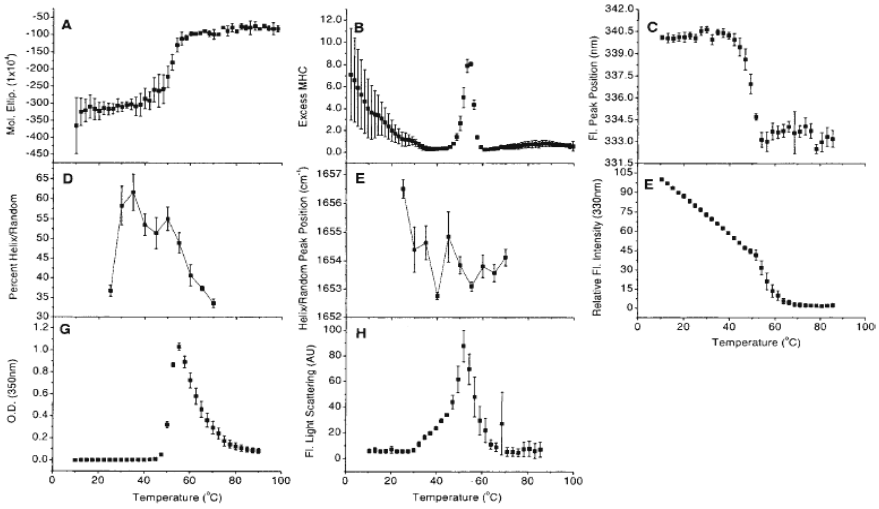

Figure 6. Characterization of bGCSF as a function of temperature at pH 7. (A) CD: ellipticity at 208 nm. (B) DSC: excess molar heat capacity. (C) Fluorescence: tryptophan peak wavelength shift. (D) FTIR: helix/random percentage. (E) FTIR: helix/random peak position. (F) Fluorescence: tryptophan emission intensity at 330 nm. (G) Temperature-induced aggregation: OD at 350 nm. (H) Rayleigh scattering during fluorescence. All errors are reported as standard error ($n = 3$).

Kueltzo L.A. and Middaugh, C.R. *J. Pharm. Sci*. (2003) **92,** 1793-1804.

Table 1. Characterization of bGCSF by CD, DSC, and Fluorescence

Method	pH	Transition Start[a] (°C)	Transition Finish[a] (°C)	Transition Midpoint[b] (°C)
CD	2	40.0	67.5	52.7 (0.1)[c]
	3	55.0	75.0	52.7 (0.1)
	4	52.5	70.0	59.9 (0.3)
	5	45.0	60.0	54.4 (0.0)
	6	47.5	60.0	53.3 (0.0)
	7	47.5	57.5	51.3 (0.0)
DSC	2	48.1	68.2	56.3
	3	51.7	72.7	64.1
	4	42.8	65.7	58.4
	5	44.8	62.3	54.9
	6	43.1	61.1	54.7
	7	43.7	60.6	53.9
Fluorescence intensity	2	24.8	56.5	48.0 (0.2)
	3	34.9	63.5	56.0 (0.3)
	4	44.6	63.8	57.6 (0.2)
	5	49.5	73.2	60.0 (0.2)
	6	52.0	68.3	57.1 (2.4)
	7	51.8	68.6	56.3 (0.3)

[a]Transition range was defined as temperatures in which values deviated from initial or terminal linear slope/baseline.
[b]Midpoints determined by fit to sigmoidal function or first derivative of the transition for non-sigmoidal events.
[c]Standard error fits to sigmoidal function for separate samples ($n = 3$).

Kueltzo L.A. and Middaugh, C.R. *J. Pharm. Sci*. (2003) **92,** 1793-1804.

Low ionic strength

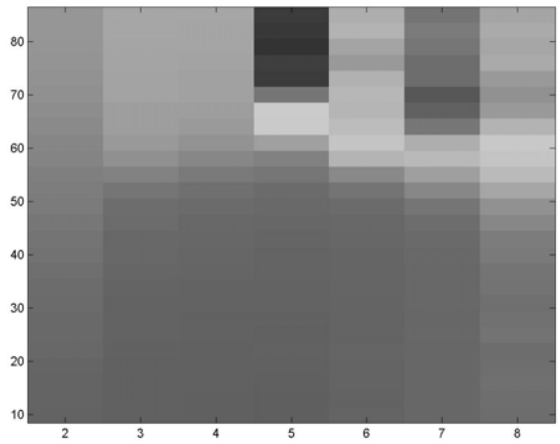

High ionic strength

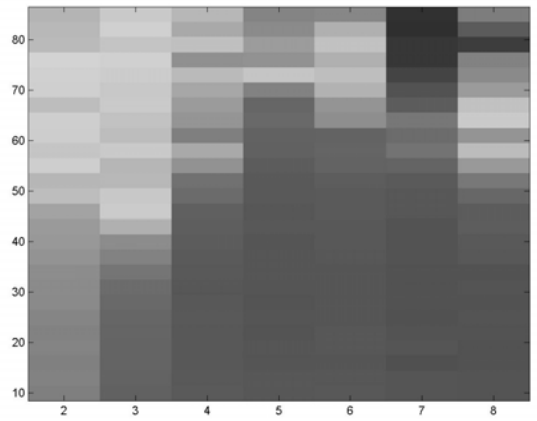

Ricin toxin A-chain

Figure 1. Second derivative UV spectrum showing the six negative peaks observed for recombinant ricin toxin A-chain.

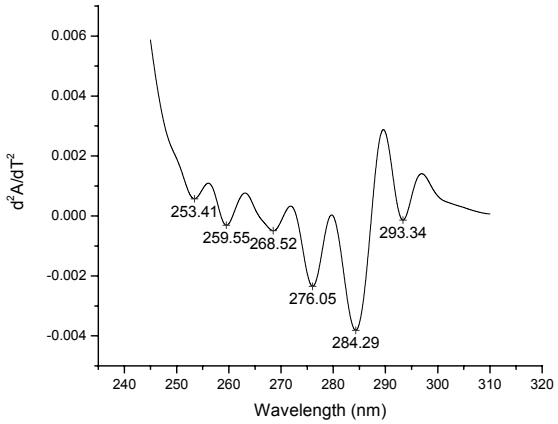

Figure 2. Shifts in second derivative UV peak position as a function of pH and temperature.

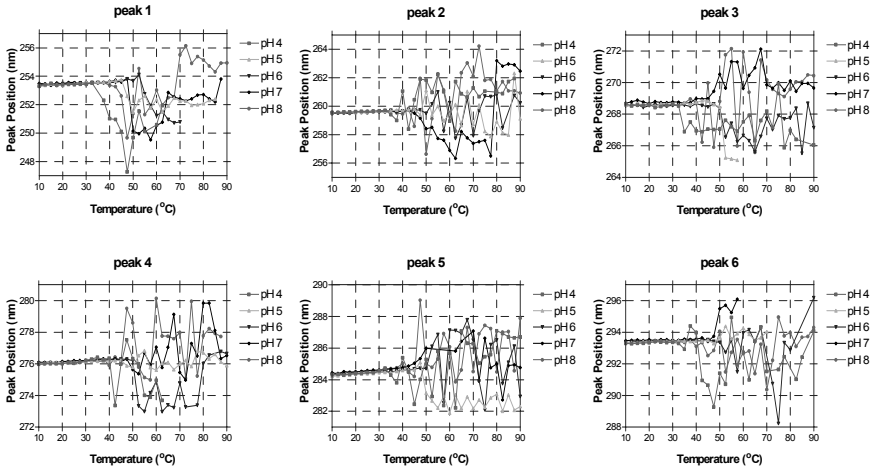

Figure 3. Phase diagram created using high-resolution second derivative UV spectroscopy data.

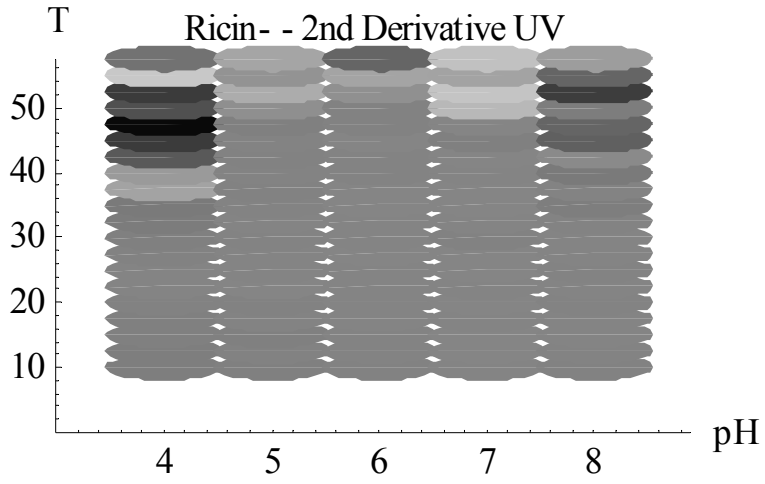

Figure 4. Turbidity of recombinant ricin toxin A-chain as a function of temperature and pH determined by high resolution second derivative UV spectroscopy.

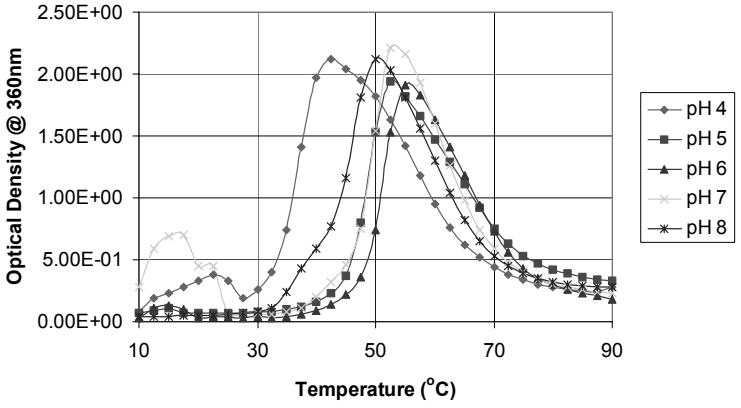

Figure 5. Effect of temperature and pH on the intrinsic Trp fluorescence intensity of recombinant ricin A-chain.

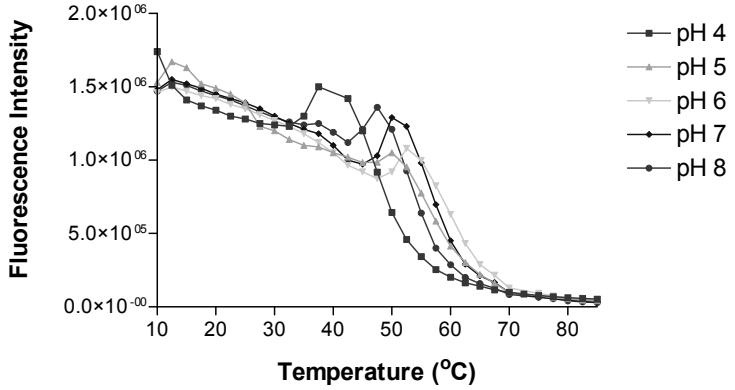

Figure 6. Effect of temperature and pH on the intrinsic Trp fluorescence peak position of recombinant ricin toxin A-chain.

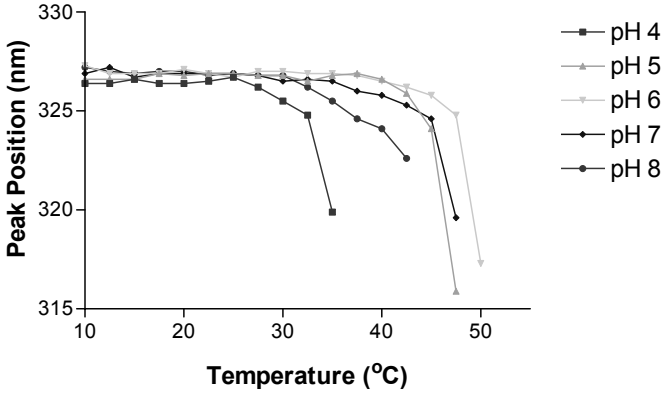

Figure 7. Circular dichroism wavelength scan at 10°C of recombinant ricin toxin A-chain

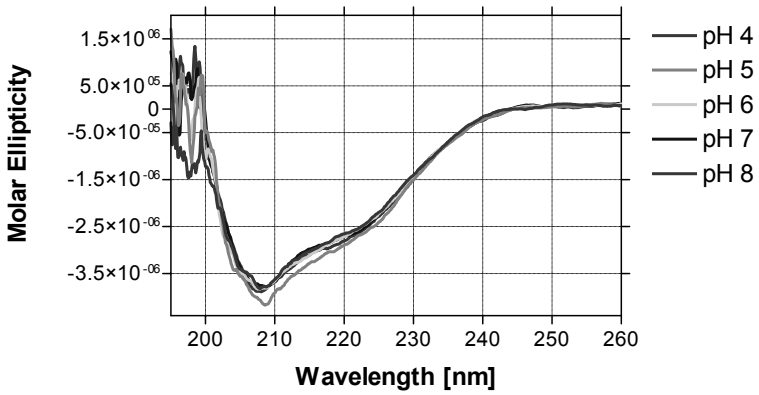

Figure 8. Circular dichroism thermal melt of recombinant ricin toxin A-chain.

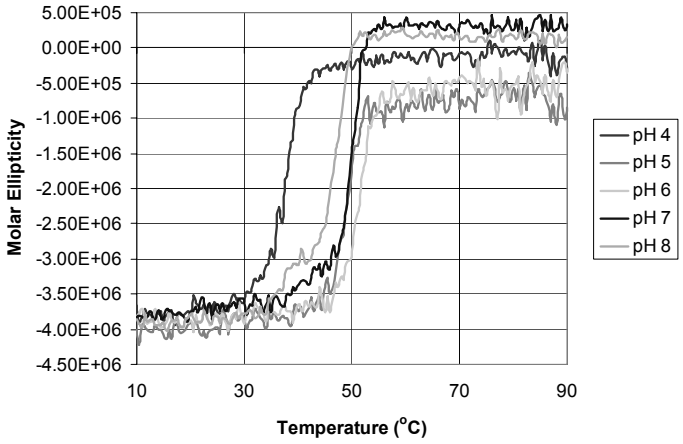

Figure 9. Effect of temperature and pH on the ANS fluorescence intensity of recombinant ricin toxin A-chain.

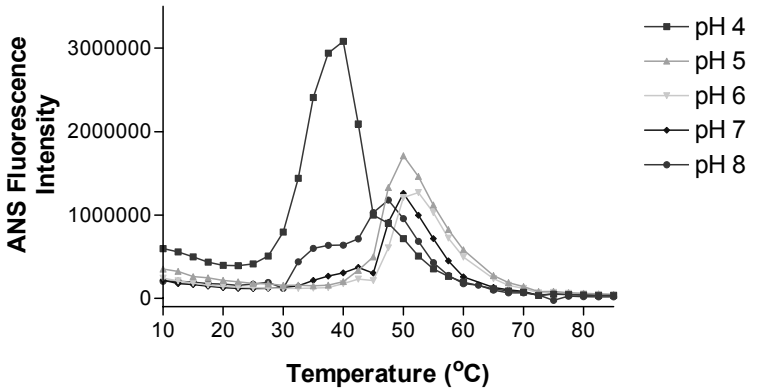

Figure 10. Effect of temperature and pH on the ANS fluorescence peak position of recombinant ricin toxin A-chain.

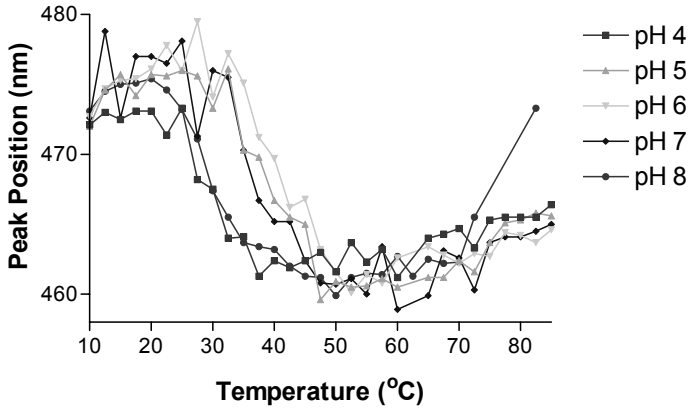

Figure 11. Phase diagram generated using ANS fluorescence and intrinsic Trp fluorescence intensity data and CD molar ellipticity data of recombinant ricin toxin A-chain.

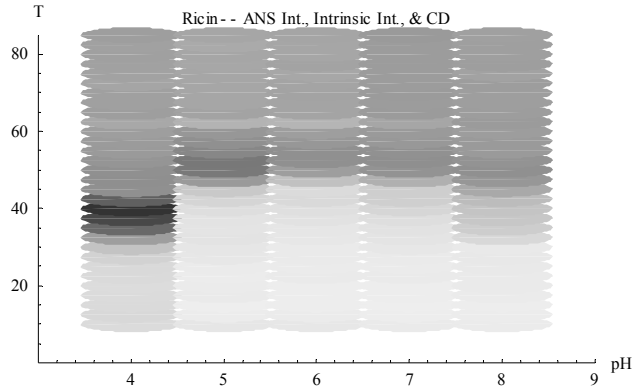

Recombinant Protective Antigen (rPA)

Fig 1. Insoluble aggregation measured at 360 nm

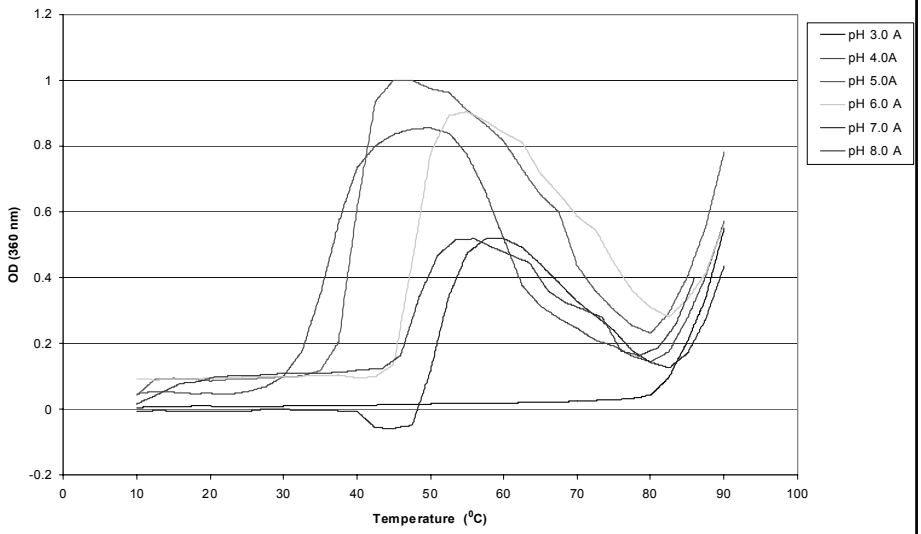

Fig 2. CD spectra of rPA at 10°C at pH 3-8 in citrate-phosphate buffer

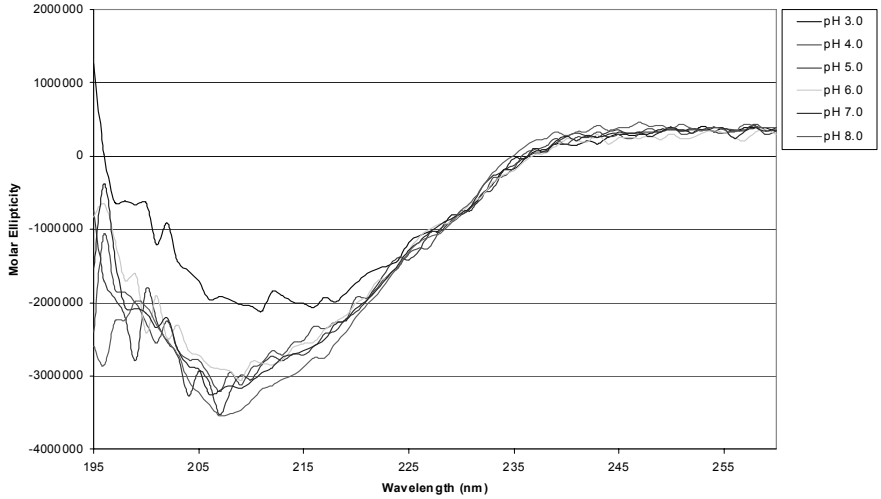

Fig 3. CD thermal melts of rPA at 222 nm at pH 3-8 in citrate-phosphate buffers

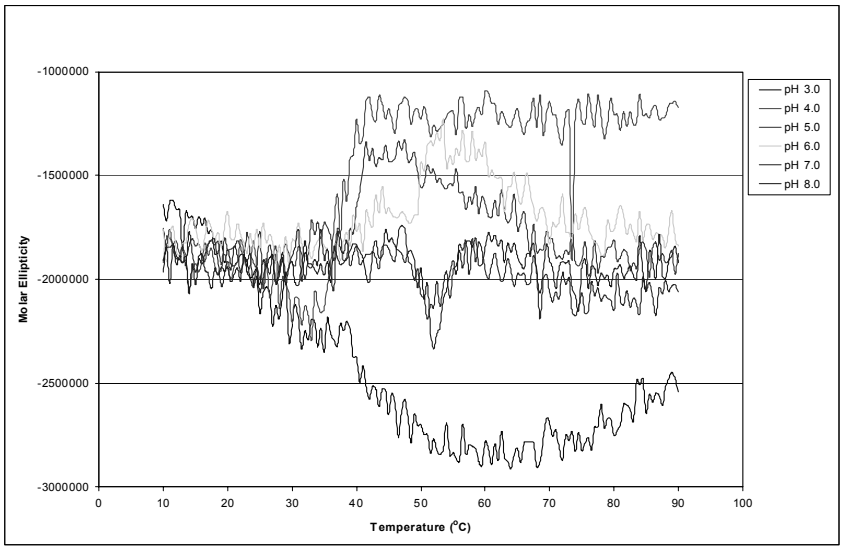

Fig 4. Effect of temperature and pH on the intrinsic Trp fluorescence

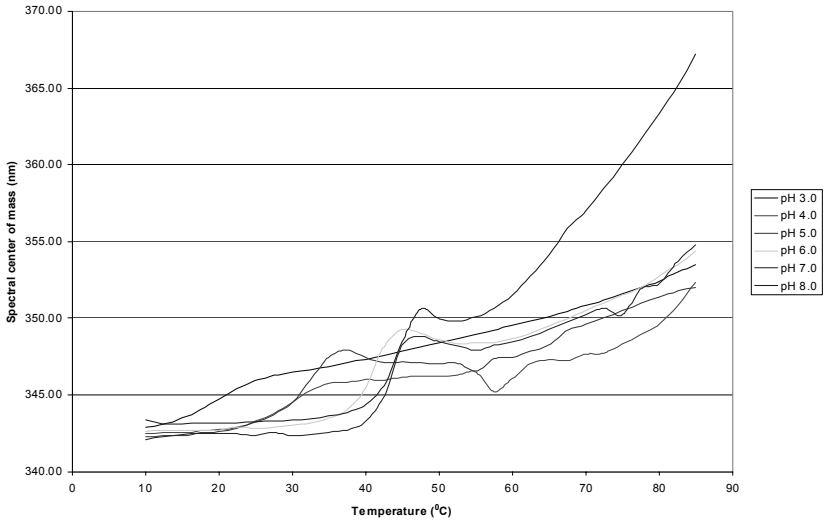

Fig 5. Effect of temperature and pH on ANS binding fluorescence intensity

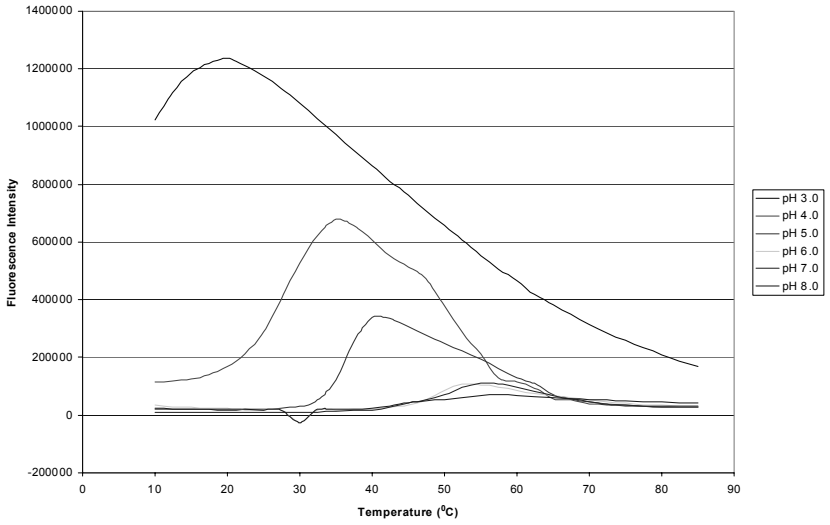

Fig 6. Phase diagram rPA based on intrinsic, ANS binding fluorescence and CD

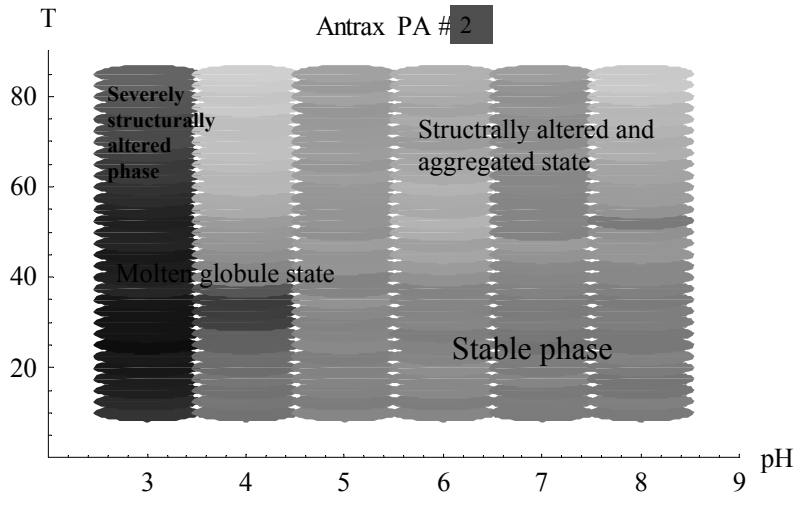

Respiratory Syncytial Virus (RSV)

Representative UV absorbance spectrum of RSV (solid line) and its second derivative (dotted line)

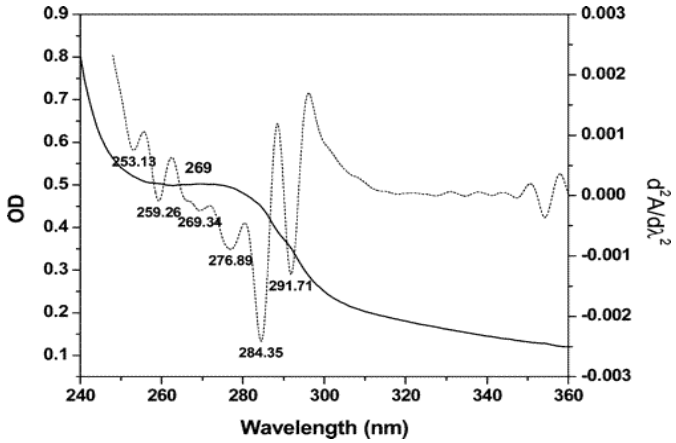

The spectrum was obtained at a viral protein concentration of 0.3 mg/mL at 10 °C, pH 7.

Ausar, et al, *Mol. Pharm.*, 2 (6), 491 -499, 2005.

High-resolution second-derivative UV spectroscopy negative peak positions as a function of temperature for RSV at pH 7

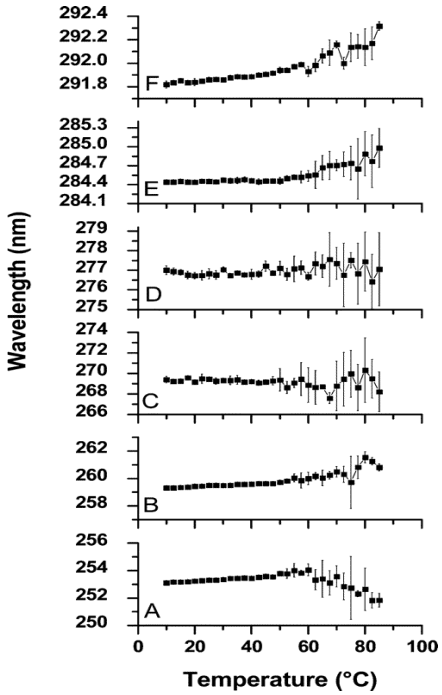

Peaks below 270 nm (A, B, and C) cannot be definitively assigned due to the overlapping absorbance of Phe and the RNA core. Peaks near 277 nm (D), 284 nm (E), and 292 nm (F) are attributed to the absorbance of Tyr, a combination of Tyr/Trp and Trp, respectively.

Ausar, et al, *Mol. Pharm.,* 2 (6), 491 -499, 2005.

Optical density at 350 nm of RSV at 10 °C as a function of pH

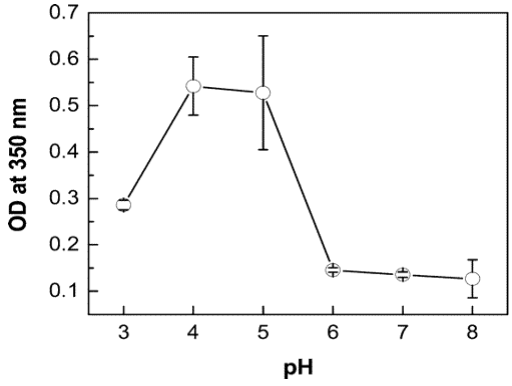

Viral protein concentration was approximately 0.3 mg/mL (*n* =3)

Ausar, et al, *Mol. Pharm.,* 2 (6), 491 -499, 2005.

Optical density at 350 nm (OD) versus temperature for RSV (0.3 mg/mL protein) at pH 3-8 (*n* = 3)

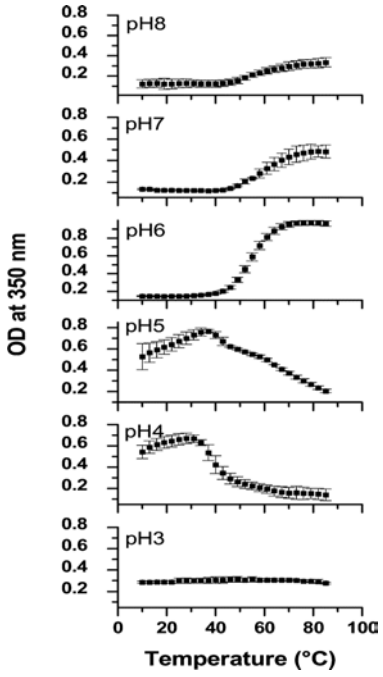

Ausar, et al, *Mol. Pharm.,* 2 (6), 491 -499, 2005.

Relative extrinsic fluorescence intensity of ANS at 485 nm versus temperature for RSV at pH 3-8

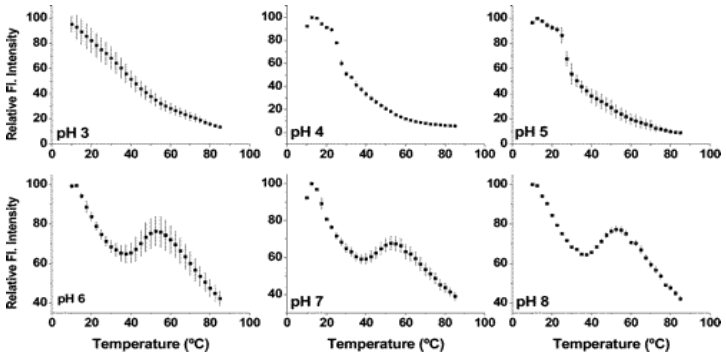

Ausar, et al, *Mol. Pharm.,* 2 (6), 491 -499, 2005.

Relative CD signal at 222 nm as a function of temperature for RSV at pH 3-8

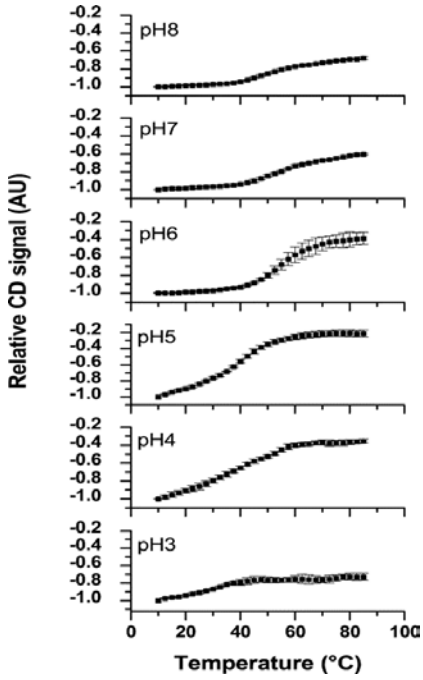

Ausar, et al, *Mol. Pharm.,* 2 (6), 491 -499, 2005.

Quaternary structural analysis of RSV by dynamic light scattering over the pH range 6-8

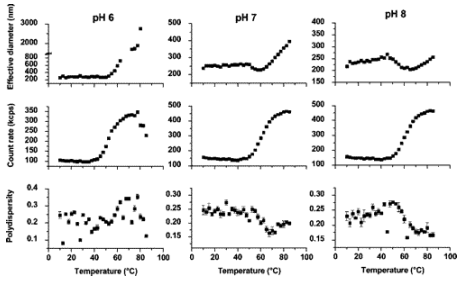

Panels are arranged from top to bottom as effective diameter, scattering count rate, and polydispersity index, respectively.

Ausar, et al, *Mol. Pharm.,* 2 (6), 491 -499, 2005.

Empirical phase diagram (EPD) of RSV over the pH range 3-8

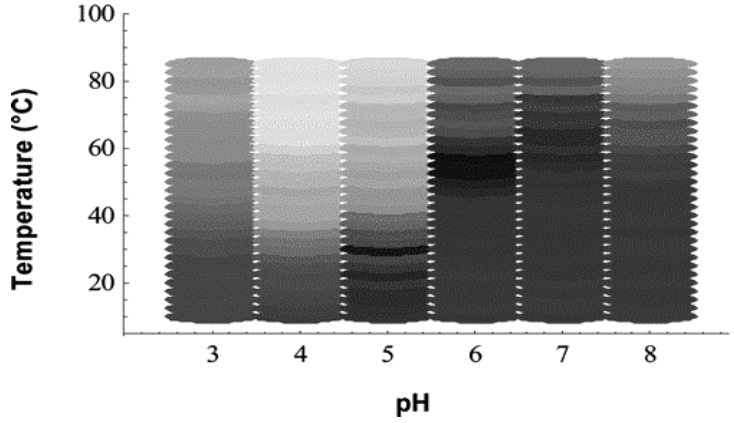

Data included in the generation of the EPD are all negative second-derivative UV peaks, CD signal at 222 nm, optical density at 350 nm, intrinsic fluorescence peak position, intrinsic fluorescence intensity at 330 nm, and ANS fluorescence intensity at 485 nm

Ausar, et al, *Mol. Pharm.,* 2 (6), 491 -499, 2005.

Norwalk Virus-like Particles (NV-VLP)

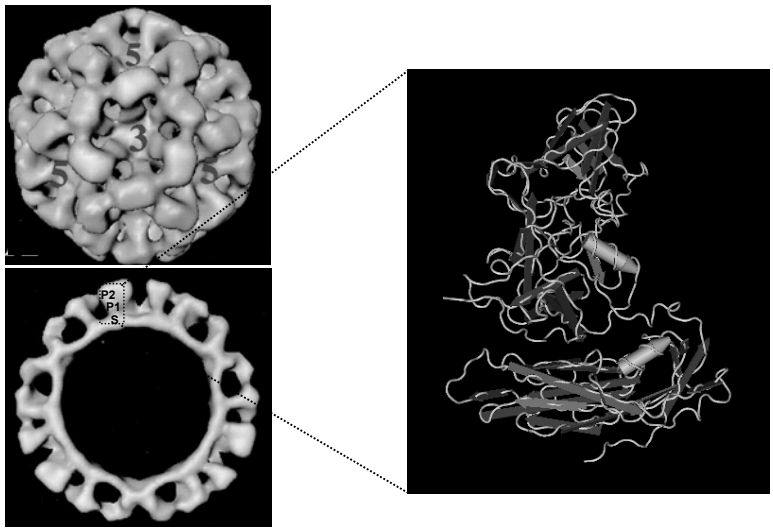

Figure 1. (A) Surface representation of 3-dimensional structure NVLP viewed along icosahedral 3-fold axes. (B) Central section along icosahedral 3-fold axis. S domains associate to form contiguous shell from which arches containing subdomains P1 and P2 emanate. (C) x-ray crystallographic structure of recombinant NV capsid protein. (Adapted from *Prasad, et al, J Infec Dis 200,181:S317-321)*

CD spectra of NV-VLPs at various pH values

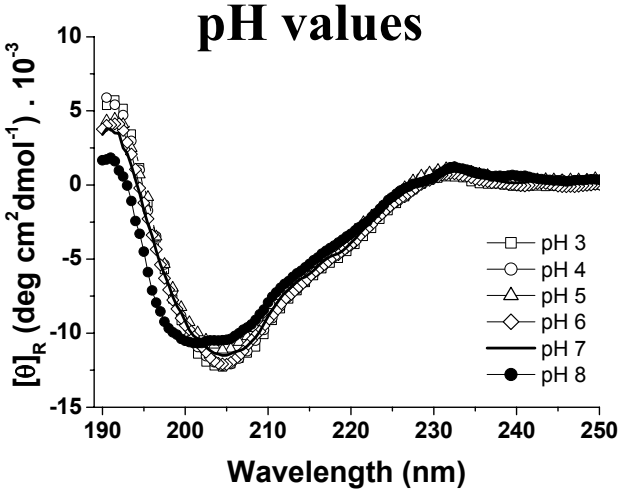

The spectra presented are an average of three consecutive scans

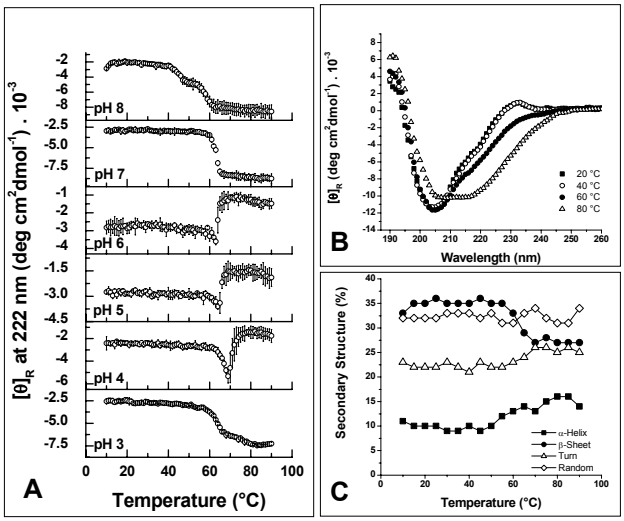

CD temperature studies of NV-VLPs. Mean residue molar ellipticity at 222 nm as a function of temperature over a range of pH 3-8 (A). The CD spectra at pH 7.0 were collected as a function of temperature (B) and the distribution of secondary structure was estimated by the program CDSSTR (C).

Second derivative UV absorbance studies of NV-VLP

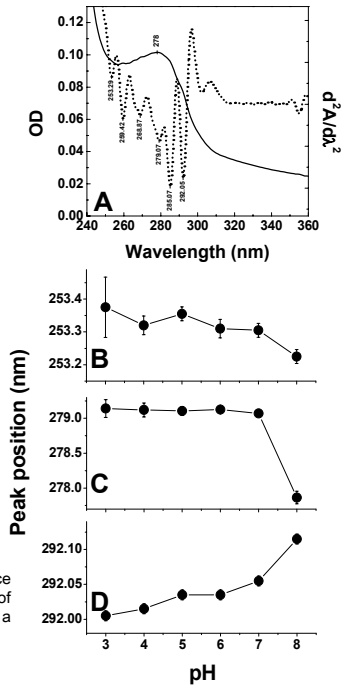

UV zero order (solid line) and second derivative (dotted line) absorbance spectra of NV-VLP at pH 7 (A). The position of the wavelength minima of phenylalaninne (B), tyrosine (C) and tryptophan (D) minima are plotted as a function of pH at 10° C. (n=3).

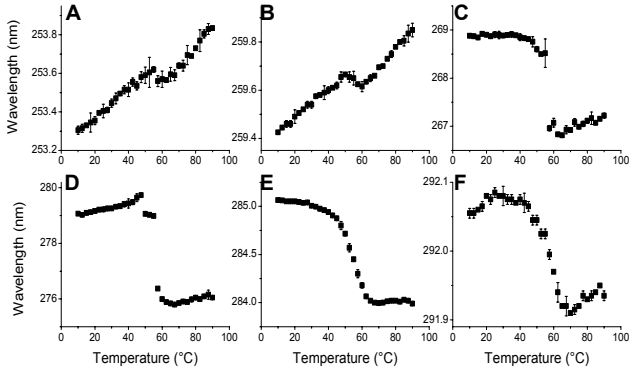

Second derivative absorbance minima arising from phenylalanine (A and B), a combination of phenylalanine and tyrosine (C), tyrosine (D), and a combination of tyrosine and tryptophan (E) and tryptophan (F) were monitored as a function of temperature at pH 7. (*n*=3).

Tryptophan emission fluorescence of NV-VLPs as a function of pH and temperature

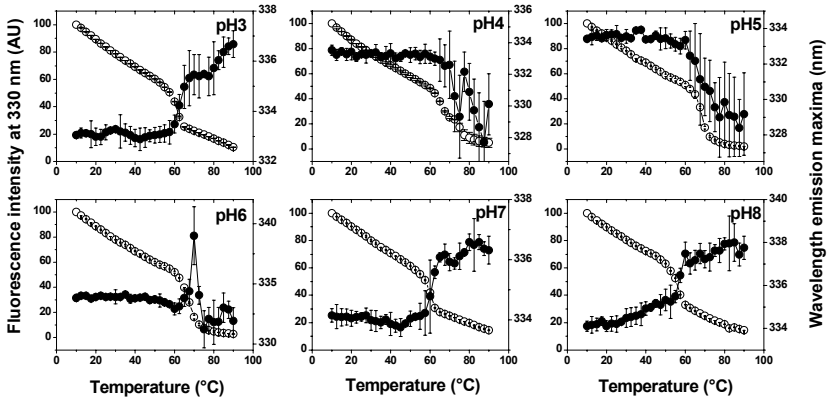

NVLPs suspensions at pH 3 to 8 were heated from 10 to 90 ° and the fluorescence emission maxima (solid circles) or the intensity at 330 nm (empty circles) were monitored. Error bars represent the standard error (*n*=3).

ANS Fluorescence intensity of NVLP as a function of pH and temperature

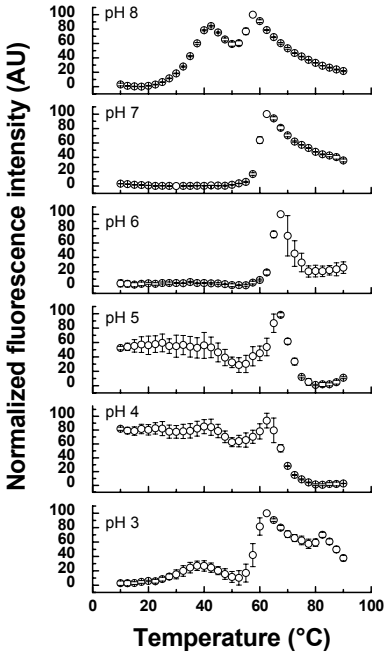

NVLPs suspensions in the presence of 40 mM 8-anilino-1-naphthalene sulfonate (ANS) were excited at 385 nm and the fluorescence intensity at 485 nm was monitored as a function of temperature at each indicated pH. Error bars represent the standard error (n=3).

Analysis of the quaternary structure of NV-VLP as a function of pH by DLS and TEM

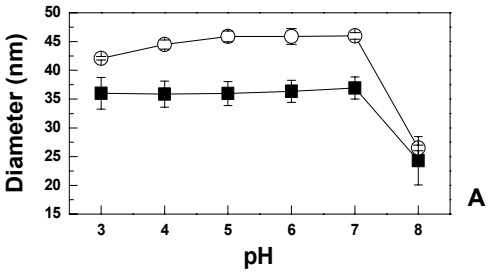

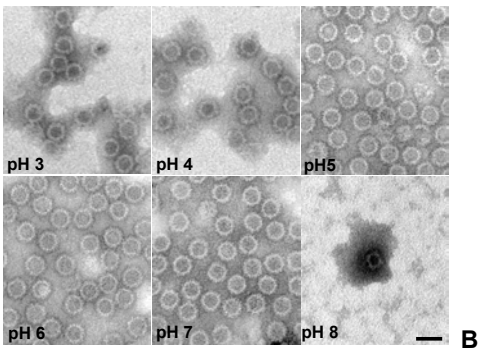

(A) NV-VLPs were dialyzed overnight against citrate/phosphate buffer at the indicated pH and the particle size was determined by DLS (open circles) or by TEM (black squares). (B) Morphology of NV-VLPs at different pH values at 10 °C using 1 % Ammonium molybdate as a negative stain. (Bar= 50nm).

Analysis of the quaternary structure of NV -VLPs as a function of pH and temperature

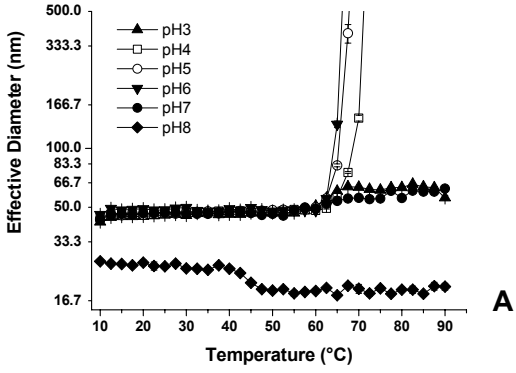

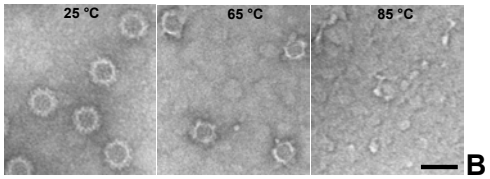

(A) The size of NV-VLPs suspended at different pH values was monitored as a function of temperature by DLS. (B) The morphology of NV-VLPs (pH 7) at different temperatures was studied by TEM using 1% Ammonium molybdate as a negative stain. (Bar= 50nm)

Empirical phase diagram for NV-VLPs based on UV, intrinsic and extrinsic fluorescence, and CD results

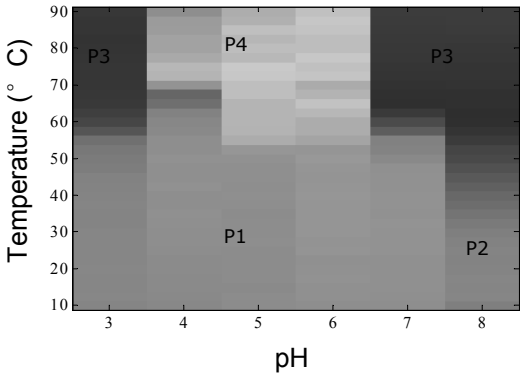

Four distinct phases (P) are observed: P1: NV-VLP in native, intact form; P2: disassembled capsids; P3: unfolded soluble capsids; P4: aggregated capsids. Blocks of continuous color represent single empirically defined phases, conditions under which raw data-derived vectors behave similarly. The colors themselves have no direct physical meaning.

DSC analysis of full length NV-VLP (panel A) and the isolated P-domain (panel B) as a function of pH

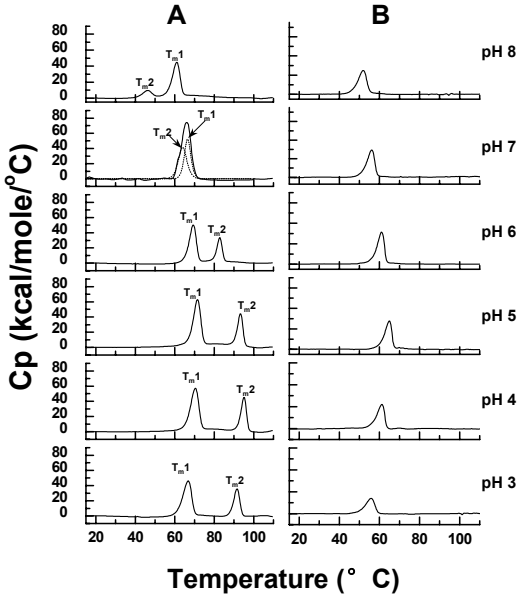

pH dependence of the transition temperatures (Tms) obtained by DSC analysis of the NV-VLP and P-domain

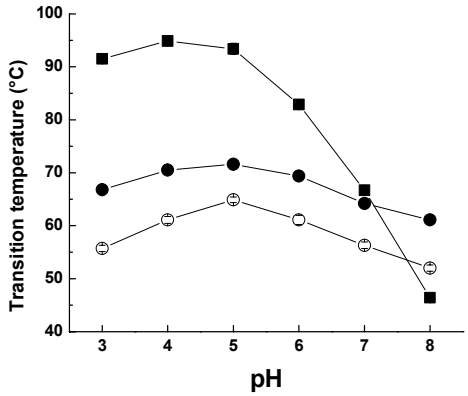

The endothermic transitions temperatures (Tm) obtained for full length NV-VLP (Tm1: black circles and Tm2: back squares) and isolated P-domain (empty circles) were plotted as a function of pH.

Other examples of Empirical Phase Diagrams

Botulinum A Holotoxin

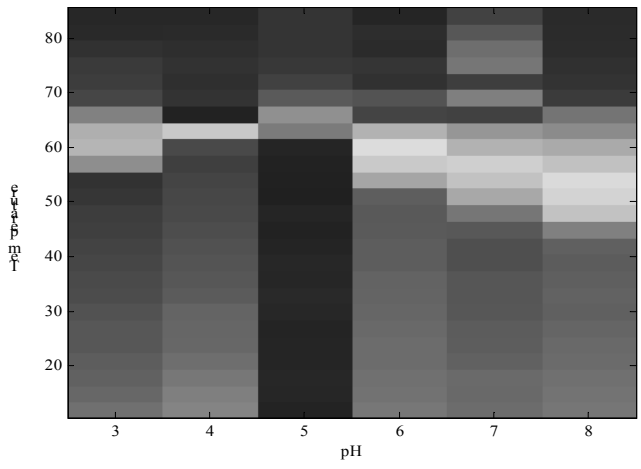

Botulinum A Neurotoxin

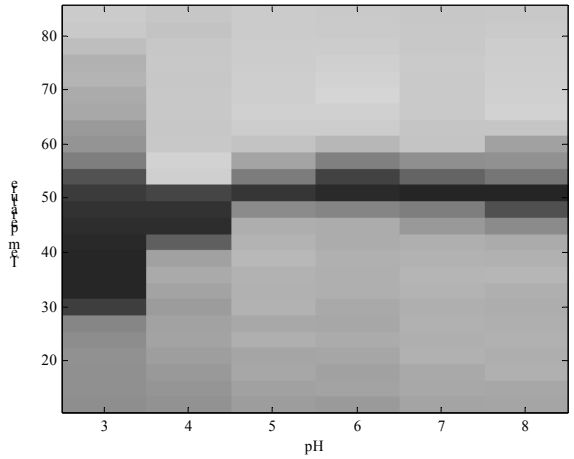

Correction Matrices for ASPs and Neurotoxin ANS Fluorescence Data (ASP+[correction]=HT)

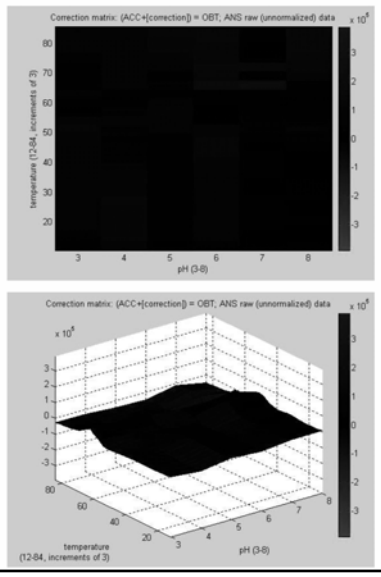

Correction Matrices for ASPs and Neurotoxin ANS Fluorescence Data (NT+[correction]=HT)

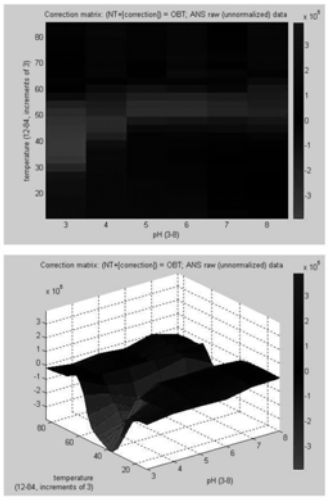

Adenovirus Type 2

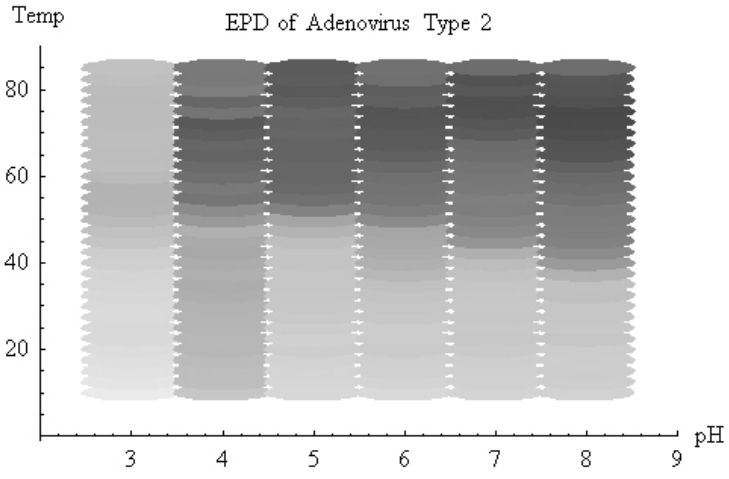

Non-Viral Gene Delivery Vehicle DOTAP

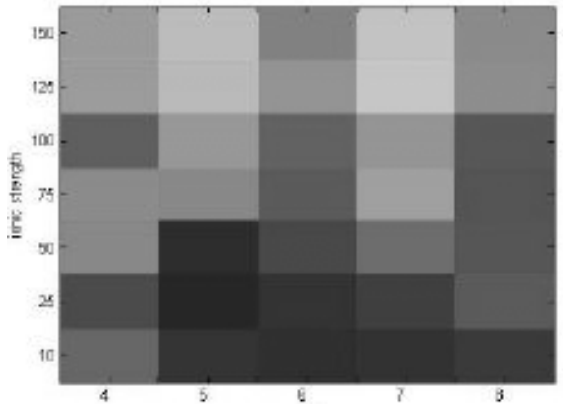

Non-Viral Gene Delivery Vehicle DOTAP (Charge ratio =4.0)

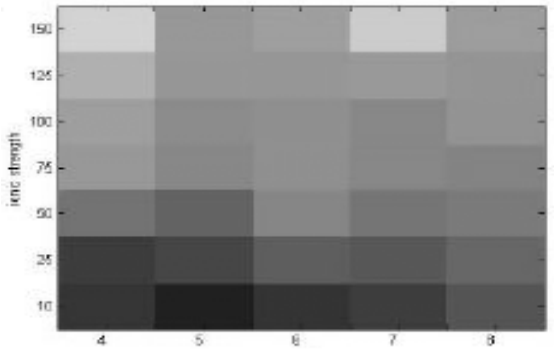

Non-Viral Gene Delivery Vehicle
DOTAP/DOPE

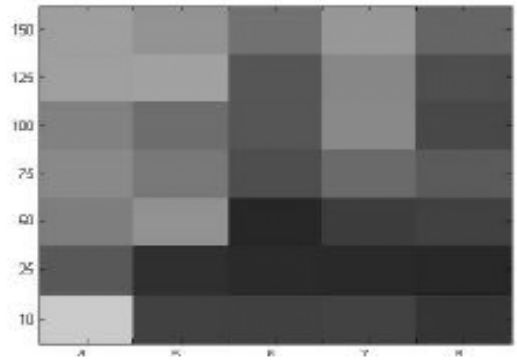

Non-Viral Gene Delivery Vehicle
DOTAP/DOPE (Charge ratio = 4.0)

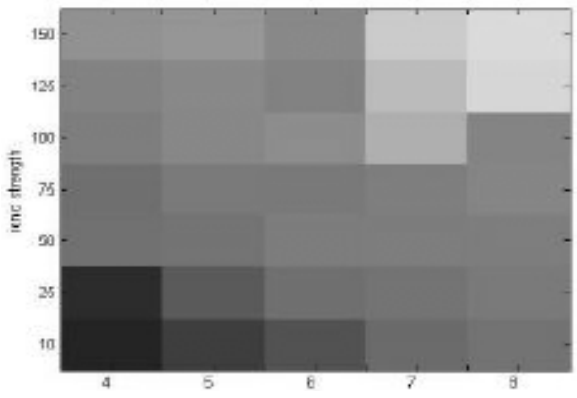

Non-Viral Gene Delivery Vehicle PLL

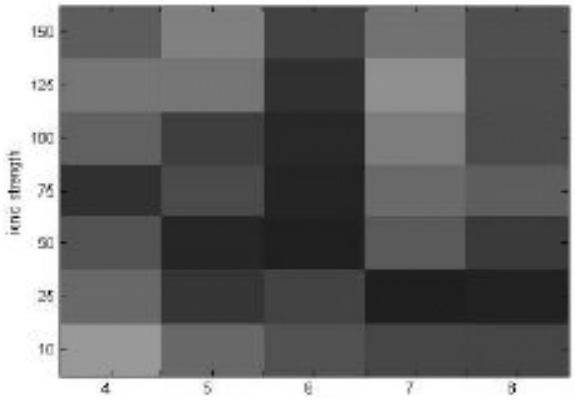

Non-Viral Gene Delivery Vehicle PLL (Charge ratio =4.0)

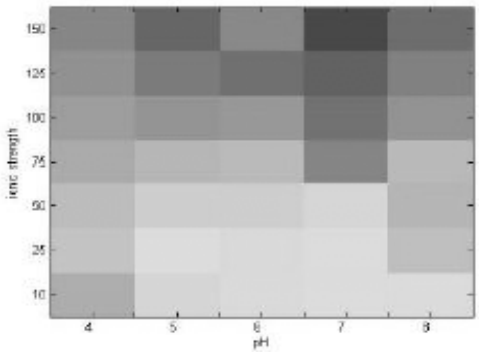

Non-Viral Gene Delivery Vehicle PEI

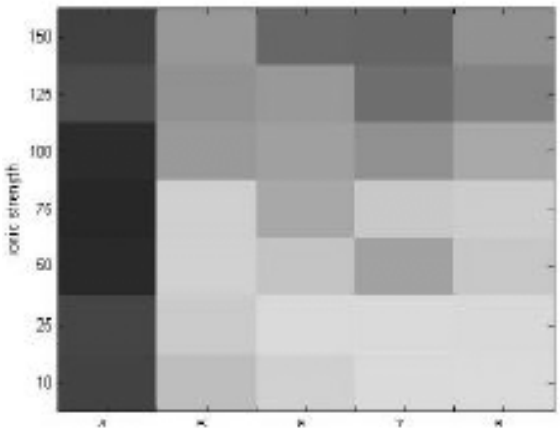

Non-Viral Gene Delivery Vehicle PEI (Charge ratio =4.0)

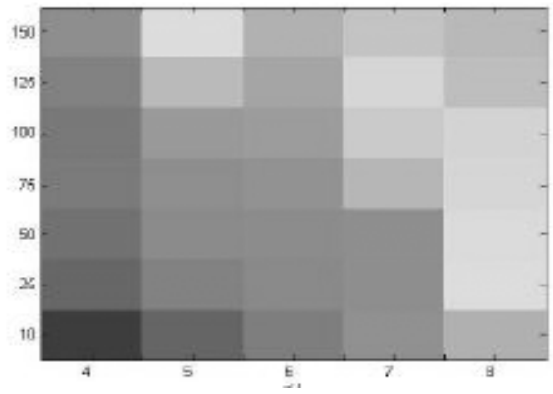

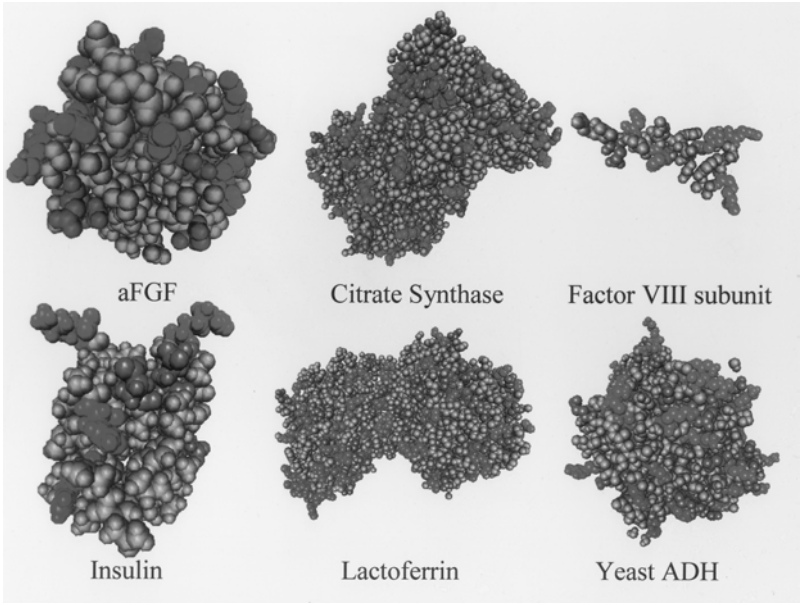

Name	Spacers
$^{+}NH_3$-$(CH_2)_n$-COO^{-}	n = 2 – 7
$^{+}NH_3$-$(CH_2)_n$-NH_3^{+}	n = 0, 2 – 7
^{-}OOC-$(CH_2)_n$-COO^{-}	n = 0 - 7
$(Gly)_n$	n = 1 – 6
Glu-Glu	
Glu-Lys	
Lys-Lys	
$^{+}NH_3$-$(Lys)^{+}$-$(Gly)_n$-$(Glu)^{-}$-COO^{-}	n = 1 – 5
$^{+}NH_3$-$(Lys)^{+}$-$(Gly)_n$-$(Lys)^{+}$-$CONH_2$	n = 1 – 5
CH_3-NH_2-$(Glu)^{-}$-$(Gly)_n$-$(Glu)^{-}$-COO^{-}	n = 1 – 5

Figure 1. Libraries screened. Each dipolar set contains either a methylene or glycine spacer (except for dimeric compounds) with at least one charge on each terminal end.

MacLean, D.S., Qian, Q., and Middaugh, C.R. *J. Pharm. Sci.,* (2002) **91**, 2220-2229.

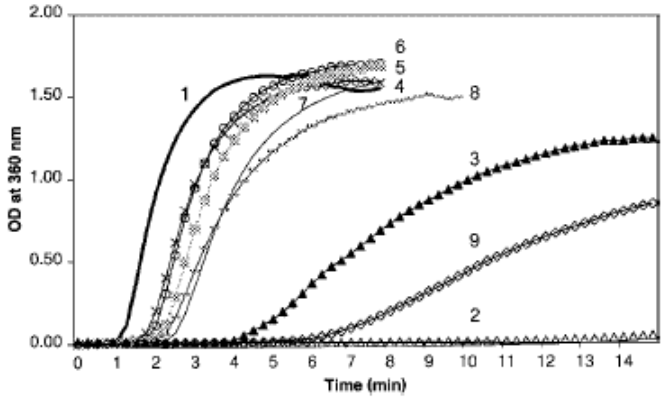

Figure 2. The effect of a 10,000× molar excess of dianions on the aggregation of 1 mg/mL (7.1 μM) yeast alcohol dehydrogenase at 37°C. 1: protein alone, 2: oxalate, 3: malonate, 4: succinate, 5: glutarate, 6: adipate, 7: pimelate, 8: suberate, 9: azelaate.

MacLean, D.S., Qian, Q., and Middaugh, C.R. *J. Pharm. Sci.,* (2002) **91**, 2220-2229.

Table 1. Effect of Multiply Charged Compounds on the Inhibition Index of Proteins

Compound	Insulin 100×	Insulin 1,000×	Lysozyme 1,000×	α-Lactalbumin 1,000×	FGF-1[a] 1,000×	FGF-1 10,000×	HLF[a] 1000×	HLF 10,000×	CS[a] 1,000×	CS 10,000×	CS 50,000×	ADH[a] 1,000×	ADH 10,000×	pST[a] 100×	pST 2,000×
Oxalate	0.9 (0.6)[a]	0.8 (0.2)[a]	1.6 (1.0)	1.3 (0.2)	5.2 (1.5)	605.5 (89.1)	N.T[a]	666.9 (314.8)	N.T.	1.9 (0.5)	6.2 (3.8)	N.T.	26.7 (3.1)	0.8 (0.1)	1.5 (0.3)
Malonate	1.2 (0.5)	0.8 (0.1)	1.5 (0.4)	1.8 (0.1)	2.2 (0.4)	36.6 (29.0)	N.T.	1714.1 (189.1)	N.T.	2.4 (0.5)	9	N.T.	18.9 (6.6)	0.9 (0.1)	4.9 (0.5)
Succinate	1.0 (0.3)	0.8 (0.2)	1.0 (0.3)	1.1 (0.3)	2.1 (0.4)	9.2 (1.9)	N.T.	33.7 (11.9)	N.T.	2.1 (0.5)	9.6	N.T.	2.7 (0.7)	0.9 (0.1)	2.1 (0.3)
Glutarate	1.0 (0.2)	0.7 (0.1)	1.2 (0.3)	1.1 (0.2)	3.0 (0.9)	10.8 (8.4)	N.T.	49.7 (28.9)	N.T.	1.4 (0.5)	6.5 (0.3)	N.T.	1.8 (0.4)	0.9 (0.1)	3.1 (0.7)
Adipate	1.2 (0.7)	0.7 (0.1)	1.4 (0.8)	1.2 (0.3)	3.0 (0.7)	5.0 (3.3)	N.T.	113.0 (119.5)	N.T.	1.2 (0.5)	19.6 (17.1)	N.T.	4.9 (0.9)	0.9 (0.1)	3.9 (0.7)
Primelate	1.4 (0.6)	0.8 (0.2)	2.0 (0.7)	1.3 (0.3)	3.1 (1.0)	12.1 (8.8)	N.T.	78.9 (68.2)	N.T.	1.4 (0.4)	6.7 (0.1)	N.T.	9.0 (1.3)	0.8 (0.1)	1.5 (0.4)
Suberate	1.6 (0.3)	0.8 (0.1)	1.4 (0.2)	2.0 (0.7)	2.3 (0.5)	7.1 (5.4)	NT.	95.4 (34.6)	N.T.	1.1 (0.2)	14.1 (2.1)	N.T.	15.5 (1.4)	0.7 (0.0)	1.7 (0.3)
Azelaate	1.5 (0.4)	0.9 (0.1)	1.0 (0.2)	2.3 (0.6)	1.9 (0.2)	6.1 (2.6)	N.T.	1455.0 (437.7)	N.T.	0.7 (0.6)	4.4 (1.8)	N.T.	40.1 (5.2)	0.6 (0.0)	1.3 (0.3)
Guanidine HCl	0.9 (0.4)	1.2 (0.3)	0.9 (0.2)	1.7 (0.6)	1.2 (0.2)	2.8 (0.9)	N.T.	0.9 (0.1)	N.T.	0.6 (0.4)	0.4 (0.1)	N.T.	0.2 (0.1)	N.T.	N.T.
Ammonium formate	1.2 (0.5)	1.0 (0.2)	1.5 (0.3)	0.8 (0.3)	0.9 (0.1)	1.3 (0.3)	N.T.	5.8 (1.1)	N.T.	0.6 (0.0)	1.2 (0.3)	N.T.	1.2 (0.1)	N.T.	N.T.
Glycine	1.0 (0.3)	0.8 (0.2)	1.0 (0.2)	1.4 (0.3)	1.3 (0.3)	3.0 (1.7)	N.T.	1.5 (0.1)	N.T.	0.8 (0.2)	N.T.	N.T.	54.3 (4.5)	0.4 (0.1)	1.2 (0.2)
Beta-alanine	1.1 (0.1)	1.0 (0.3)	1.1 (0.3)	2.1 (0.4)	1.1 (0.2)	1.5 (0.5)	N.T.	24.2 (1.4)	N.T.	0.6 (0.1)	1.9 (0.8)	N.T.	2.2 (0.3)	0.4 (0.1)	0.8 (0.1)
4-Aminobuytrate	1.2 (0.3)	0.8 (0.0)	1.4 (0.4)	2.0 (0.8)	1.5 (0.0)	1.4 (0.3)	N.T.	9.5 (1.9)	N.T.	0.7 (0.1)	1.2 (0.4)	N.T.	2.0 (0.1)	0.3 (0.0)	1.1 (0.2)
5-Aminovalerate	1.2 (0.1)	0.9 (0.1)	1.5 (0.4)	2.1 (0.8)	1.1 (0.2)	2.2 (1.4)	N.T.	8.4 (2.6)	N.T.	0.7 (0.1)	1.9 (0.7)	N.T.	2.7 (0.9)	0.4 (0.0)	0.7 (0.1)
6-Aminocaproate	1.4 (0.2)	0.9 (0.1)	0.8 (0.2)	2.3 (0.6)	2.2 (0.3)	2.4 (0.5)	N.T.	7.9 (3.4)	N.T.	0.5 (0.1)	1.5 (0.8)	N.T.	3.2 (0.3)	0.5 (0.1)	1.2 (0.2)
7-Aminoheptanoate	2.4 (1.0)	1.1 (0.2)	1.3 (0.2)	3.9 (2.1)	0.9 (0.4)	1.3 (0.1)	N.T.	4.7 (0.7)	N.T.	0.5 (0.1)	1.7 (0.4)	N.T.	4.9 (0.5)	0.4 (0.0)	1.6 (0.2)
Hydrazine	0.9 (0.4)	1.0 (0.2)	12.2 (6.0)	0.5 (0.5)	1.6 (0.6)	7.0 (3.2)	N.T.	16.0 (6.2)	N.T.	0.9 (0.2)	6.8	N.T.	0.3 (0.1)	N.T.	N.T.
Ethylenediamine	0.9 (0.3)	1.3 (0.3)	70.2 (6.8)	0.7 (0.4)	2.2 (0.7)	3.3 (1.3)	N.T.	44.5 (13.9)	N.T.	1.8 (0.5)	18.5	N.T.	202.6 (69.7)	0.7 (0.0)	1.3 (0.1)
1,3-Diaminopropane	1.3 (0.3)	1.4 (0.3)	2.7 (0.4)	0.9 (0.3)	2.2 (0.3)	3.5 (2.3)	N.T.	31.5 (12.0)	N.T.	0.7 (0.3)	7.7	N.T.	0.7 (0.1)	0.6 (0.0)	1.7 (0.2)
1,4-Diaminobutane	1.4 (0.4)	1.3 (0.2)	1.6 (0.2)	1.0 (0.2)	2.5 (1.3)	33.7 (6.6)	N.T.	34.5 (13.0)	N.T.	0.9 (0.3)	4.0 (2.3)	N.T.	0.8 (0.1)	0.6 (0.1)	1.4 (0.4)
1,5-Diaminopentane	1.5 (0.6)	1.2 (0.1)	1.3 (0.3)	0.9 (0.0)	3.3 (0.7)	46.5 (19.8)	N.T.	28.8 (13.3)	N.T.	0.8 (0.2)	8.3 (4.5)	N.T.	0.9 (0.0)	0.8 (0.3)	1.7 (0.4)
1,6-Diaminohexane	1.5 (0.3)	1.5 (0.2)	1.0 (0.1)	1.3 (0.4)	1.6 (0.6)	27.0 (9.8)	N.T.	18.0 (4.9)	N.T.	0.6 (0.2)	4.8 (1.5)	N.T.	0.8 (0.0)	0.6 (0.1)	1.9 (0.2)
1,7-Diaminohexane	2.7 (1.0)	1.3 (0.2)	1.0 (0.3)	1.8 (0.7)	2.0 (0.7)	6.2 (2.4)	N.T.	11.0 (2.1)	N.T.	0.6 (0.2)	1.7 (0.7)	N.T.	0.6 (0.1)	1.7 (0.0)	1.6 (0.7)
Glu-Glu	1.0 (0.1)	0.6 (0.1)	1.2 (0.7)	1.0 (0.1)	1.3 (0.2)	7.1 (2.7)	9.8 (0.8)	2.1	0.8 (0.1)	1.5 (0.1)	1430.3	1.4 (0.2)	5.3 (1.2)	0.6 (0.1)	N.T.
Glu-Lys	1.0 (0.1)	0.8 (0.1)	1.0 (0.4)	1.0 (0.1)	1.6 (0.3)	11.0 (3.0)	9.8 (0.3)	44.5	0.8 (0.2)	1.6 (0.2)	21.5	1.7 (0.1)	18.4	N.T.	N.T.
Lys-Lys	1.1 (0.1)	0.9 (0.3)	1.3 (0.1)	1.0 (0.1)	1.1 (0.1)	3.1 (0.8)	13.5 (1.2)	11.2	0.9 (0.1)	1.6 (0.3)	86.8	1.4 (0.2)	2.7	0.9 (0.1)	1.9 (0.3)
Diglycine	1.0 (0.2)	0.8 (0.1)	0.9 (0.0)	1.0 (0.0)	1.0 (0.1)	1.2 (0.4)	7.4 (1.0)	10.0	0.8 (0.1)	0.9 (0.3)	30.3	1.5 (0.2)	4.0 (0.9)	0.7 (0.1)	N.T.
Triglycine	1.4 (0.1)	0.8 (0.4)	1.6 (0.3)	0.9 (0.1)	2.2 (1.1)	3.1 (0.9)	0.2 (0.1)	5.7 (4.0)	1.0 (0.2)	0.7 (0.2)	1.0	6.0 (1.4)	187.6 (46.1)	0.7 (0.0)	2.5 (0.3)
Tetraglycine	1.5 (0.3)	N.T.	2.1 (0.5)	1.3 (0.4)	3.8 (0.8)	N.T.	8.3 (9.5)	0.1	1.5 (0.1)	N.T.	N.T.	8.4 (2.7)	5313.1	0.8 (0.1)	3.4 (0.6)
Pentaglycine	1.0 (0.2)	N.T.	0.2 (0.1)	3.1 (1.2)	N.T.	N.T.	979.0 (7.5)	0.5 (0.0)	0.6 (0.2)	N.T.	N.T.	5.8 (3.1)	Infinite[a]	0.7 (0.2)	N.T.
Hexaglycine	1.5 (0.7)	N.T.	0.0 (0.0)	4.2 (1.1)	N.T.	N.T.	1.7 (1.5)	N.T.	0.5 (0.1)	N.T.	N.T.	1.7 (0.5)	20.3	0.7 (0.1)	N.T.

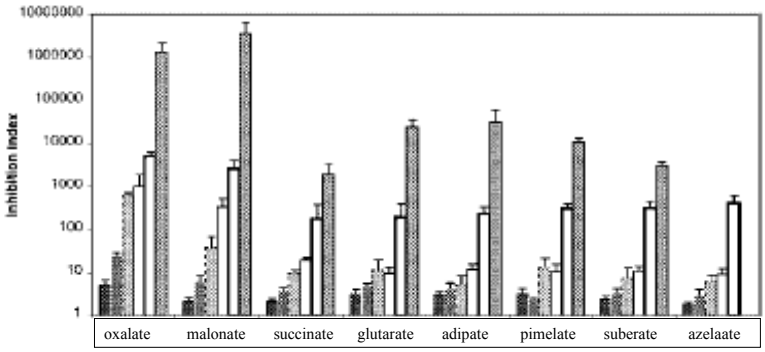

Figure 3. The effect of dianion concentration on the inhibition of FGF-1 aggregation. A 50-μg/mL solution of FGF-1 in PBS was monitored at 50°C. Starting from left to right for the series of bars corresponding to each protein, ligand concentrations are 1000×, 5000×, 10,000×, 12,500×, 25,000×, and 50,000×.

MacLean, D.S., Qian, Q., and Middaugh, C.R. *J. Pharm. Sci.,* (2002) **91**, 2220-2229.

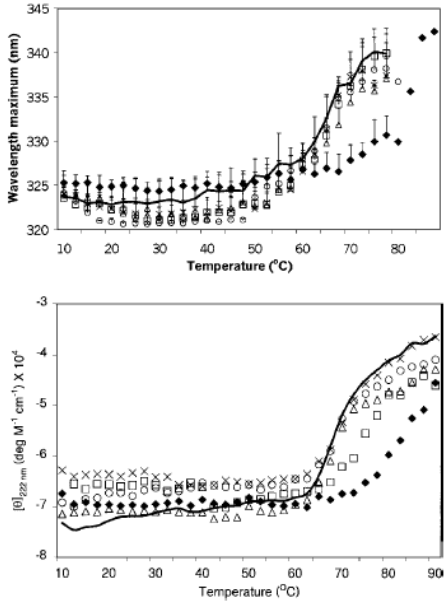

Figure 4. Effect of temperature on the CD (222 nm) and fluorescence emission maximum of apo HLF at a 10,000× molar excess of oxalate (◆), malonate (△), glycine (×), beta-alanine (□), and ethylenediamine (○). The protein in the absence of compounds is shown as a solid line (—) without symbol.

MacLean, D.S., Qian, Q., and Middaugh, C.R. *J. Pharm. Sci.,* (2002) **91**, 2220-2229.

Table 2. Spectral Transition Temperatures (T_ms,°C) (±SD) for Alcohol Dehydrogenase, Apolactoferrin, and Lysozyme in the Presence of Various Ligands

	ADH		HLF		Lysozyme	
	CD	Fluorescence	CD	Fluorescence	CD	Fluorescence
None	58.7 (0.6)	57.3 (0.3)	71.0 (1.2)	65.6 (1.8)	73.4 (1.2)	71.5 (1.6)
Oxalate	59.7 (0.6)	54.6 (2.6)	81.5 (2.6)[a]	79.5 (5.3)[a]	72.8 (1.5)	72.8 (0.8)[a]
Malonate	60.3 (2.3)	56.3 (1.2)	68.7 (1.0)[b]	66.6 (3.0)	72.9 (0.7)	75.9 (0.6)[a]
Glycine	59.3 (0.6)	55.8 (1.4)	70.5 (2.2)	66.3 (1.3)	73.8 (1.0)	71.8 (0.7)
Beta-alanine	59.9 (0.3)[a]	58.6 (1.3)	75.4 (1.5)[a]	67.2 (0.6)	73.2 (0.3)	71.8 (1.4)
Ethylenediamine	60.5 (0.5)[a]	58.7 (1.3)	69.5 (0.9)	65.8 (0.7)	75.0 (0.3)	70.1 (1.7)

The CD thermal transition was monitored at 222 nm. The fluorescence thermal transition was determined by the shift in the wavelength emission maxima. [ADH] = 1.59E-6M for CD and 6.64E-7M for fluorescence. [HLF] = 1.05E-6M for CD and 4.36E-7M for fluorescence. [lysozyme] = 7.74E-6M for CD and 2.75E for fluorescence. Fluorescence measurements were obtained at 2.5°C intervals after equilibration at each temperature.

[a]Delays initiation of thermal transition.

[b]Hastens initiation of thermal transition.

MacLean, D.S., Qian, Q., and Middaugh, C.R. *J. Pharm. Sci.,* (2002) **91**, 2220-2229.

Table 3. The Effect of Terminally Charged Ligands on Selected Protein's Relative Activities

Compound	ADH 10,000×	Lysozyme 10,000×	Citrate Synthase 10,000×	50,000×
None	1.00 (0.02)	1.00 (0.05)	1.00 (0.02)	NA
Oxalate	0.99 (0.13)	1.30 (0.02)[a]	0.90 (0.01)[a]	0.90 (0.06)
Malonate	0.93 (0.07)	1.36 (0.04)[a]	1.26 (0.14)[a]	0.82 (0.02)[a]
Glycine	1.12 (0.03)[a]	1.17 (0.03)[a]	1.14 (0.14)	ND
Beta-alanine	0.98 (0.08)	1.24 (0.02)[a]	ND	ND
Ethylenediamine	1.40 (0.04)[a]	2.55 (0.02)[a]	0.93 (0.06)	1.05 (0.05)

ND—Not done.

NA—not applicable.

[a]Significant difference ($P < 0.05$).

MacLean, D.S., Qian, Q., and Middaugh, C.R. *J. Pharm. Sci.,* (2002) **91**, 2220-2229.

Table 1. Inhibition of rPA thermal aggregation at 37°C by various GRAS excipients

Excipient	Molar ratio (Excipient: PA), Molarity (excipient) or wt. Percent (Excipient)	% Inhibition
Sorbitol	20.00%	106
Mannitol	10.00%	100
Sodium Citrate	0.2 M	95
Sodium Citrate	0.1 M	94
Trehalose	20.00%	94
Dextrose	10.00%	93
Histidine	0.3 M	88
Dextrose	20.00%	85
Malic Acid	0.15 M	83
Dietanolamine	0.3 M	62
Sucrose	20.0%	59
Glycerol	10.00%	48
Sucrose	10.00%	46
Tween 80	0.10%	46
Brij 35	0.01%	41
$CaCl_2$	0.015 M	40
Tween 20	0.10%	14
2-OH propyl β-CD	5.00%	14
Dextran T40	0.1	12
α Cyclodextrin	2.50%	6
Albumin	1.00%	0
Pluronic F-68	0.05%	-14

Fig 7. Protection against rPA aggregation by trehalose

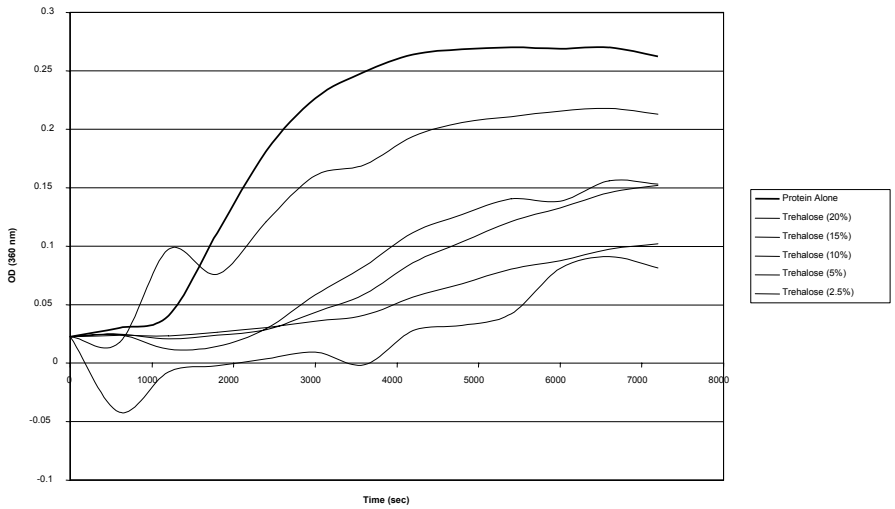

Fig 8. Increase of rPA thermal transition temperature by trehalose in comparison to some other excipients

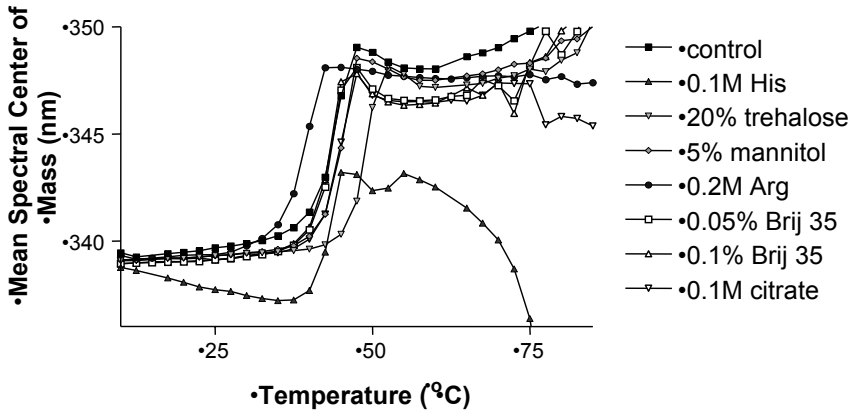

Inhibition of Aggregation of recombinant ricin toxin A-chain V76M/Y80A at 45°C by various GRAS excipients

	% Inhibition
Pluronic F-68 (0.1%)	93%
Brij 35 (0.1%)	* 89%
Glycine (0.3M)	82%
Histidine (0.3M)	81%
Lysine (0.3M)	79%
Pluronic F-68 (0.05%)	78%
Glycerol (20%)	78%
Dextrose (20%)	77%
Sucrose (20%)	76%
Proline (0.3M)	75%
Gelatin (5%)	73%
Brij 35 (0.05%)	* 73%
Brij 35 (0.01%)	* 71%
Sorbitol (10%)	70%
Arginine (0.3M)	70%
Lactose (20%)	69%
Sucrose(10%)	68%
Trehalose (20%)	67%
Heparan Sulfate (10x)	67%

Dietanolamine (0.3M)	67%
2-OH propyl γ-CD (5%)	66%
Gelatin (2.5%)	65%
2-OH propyl β-CD (10%)	65%
SOS (10x)	64%
Dextrose (10%)	64%
Trehalose (10%)	63%
Sorbitol(20%)	63%
Guanidine (0.3M)	63%
Glycerol (10%)	63%
Pluronic F-68 (0.01%)	62%
Mannitol (10%)	62%
2-OH propyl γ-CD (10%)	62%
2-OH propyl β-CD (5%)	60%
Heparin (10x)	58%
Phytic Acid (10x)	55%
Malic Acid (0.15M)	51%
Lactose (10%)	51%
Lactic Acid (0.15M)	49%
α Cyclodextrin (2.5%)	44%

Glu + Arg (0.05M each)	43%
Dextran Sulfate (10x)	42%
Lactose (1.7%)	36%
Heparin (1x)	13%
Sucrose Octasulfate (0.1x)	12%
Tween 80 (0.1%)	12%
Dextran Sulfate (0.1x)	10%
Tween 80 (0.05%)	10%
Dextran Sulfate (1x)	9%
Tween 80 (0.01%)	5%
Heparan Sulfate (1x)	3%
Phytic Acid (1X)	2%
Phytic Acid (0.1X)	2%
Heparin (0.1x)	2%
Heparan Sulfate (0.1x)	2%
Ascorbic acid (0.15M)	AGG
Tween 20 (0.1%)	-13%
Tween 20 (0.05%)	-56%
Tween 20 (0.01%)	-86%
SOS (1x)	-10

*An initial increase in OD_{360} was observed.

Inhibition of RSV aggregation kinetics at 56°C by various excipients

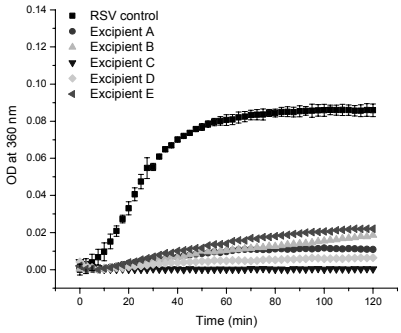

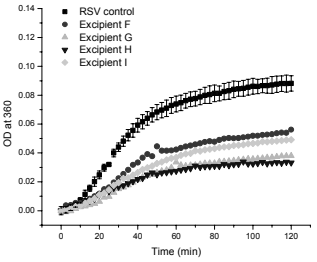

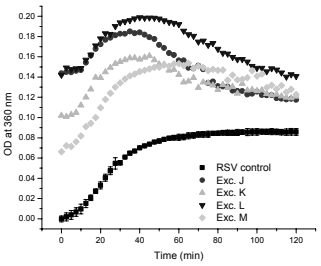

Effect of various excipients on the aggregation kinetics of RSV. The excipient concentrations are indicated in each plot. For clarity reasons only the error bars for the control experiment are shown. All of the experiments were performed in triplicate.

Increase of the thermal transition of RSV by various GRAS excipients

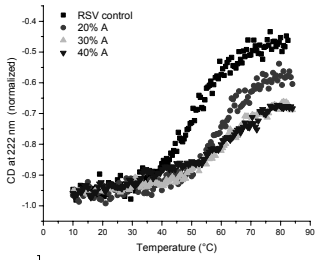

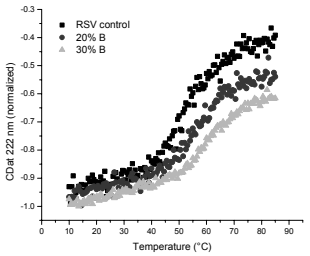

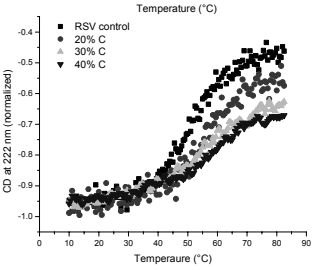

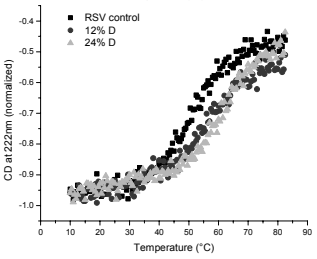

CD thermal melts of RSV samples in the presence of stabilizers was monitored at 222 nm. A thermal melt of RSV samples without excipients (control) is also shown

A Generic Approach to the Identification of Stabilizers of Macromolecules

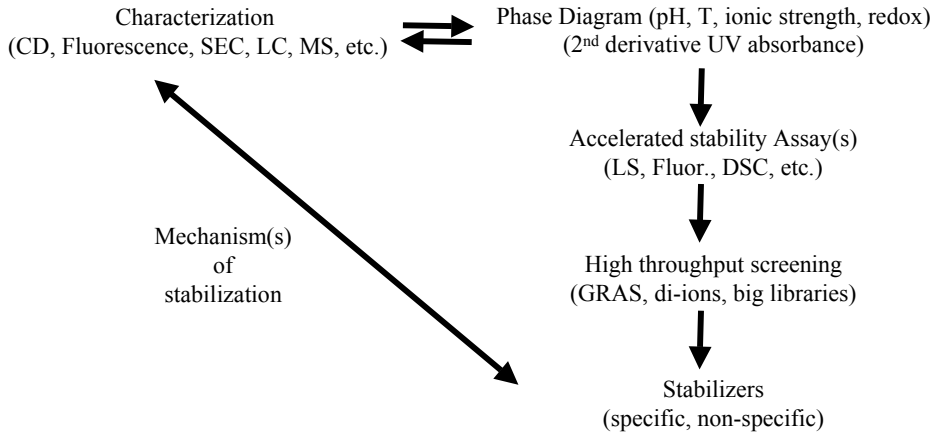

Acknowledgements

Lisa Kueltzo
LaToya Jones
Haihong Fan
Fernando Ausar
Laura Peek
Sangeeta Joshi
John Ralston
Donald MacLean
Quansheng Qian

Pfizer – Todd Derrington
BD Technologies – Kevin Mar
Dor BioPharma – Ellen Vitteta / Rob Brey
DOD
Thrasher Foundation
NIH

Factor VIII

(A) HP-SEC analysis of rhFVIII samples showing formation of aggregates with time. The data for the incubation time points have been stacked for easy visualization. From top to bottom: 0 h, 6 h, 1 day, 2 day, 3 day, 4 day, 5 day, 6 day, and 7 day incubation time points. Gel filtration performed in 50 mM Tris, 400 mM NaCl, 5mM CaCl2, 0.05% NaN3, pH 7.0. The flow rate was 0.65mL/min

(B) Dynamic light scattering analysis of rhFVIII samples as a function of incubation time. The mean diameters obtained by second-order cumulant (triangles) and NNLS (circles) analysis are shown. Protein concentration was ~0.1mg/mL.

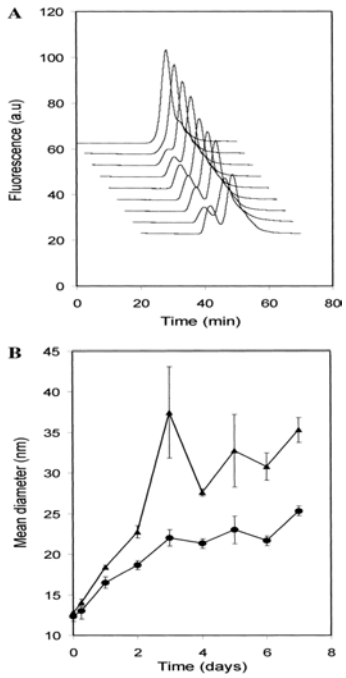

Grillo et al. *Biochemistry*, 40 (2), 586 -595, 2001

Biological Activity and Extent of Aggregation of RhFVIII Samples as a Function of Incubation Time at 37 °C

time	% activity	% aggregation
0 h	100	0
6 h	101	0
1 day	96	10
2 days	97	15
3 days	90	20
4 days	92	20
5 days	89	20
6 days	92	18
7 days	85	26

[a] Activity was determined from a one-stage activated partial thromboplastin time assay

Grillo et al. *Biochemistry*, 40 (2), 586 -595, 2001

(A) Far-UV CD spectrum of rhFVIII at 25 °C. (B) Fluorescence emission spectra of fractionated native (13.25 μg/mL, circles) and aggregate (19.17 μg/mL, triangles) species in 25 mM Tris, 300 mM NaCl, 4 mM CaCl2, pH 7

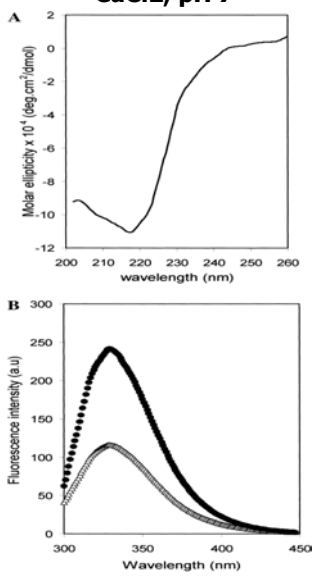

Grillo et al. *Biochemistry*, 40 (2), 586 -595, 2001

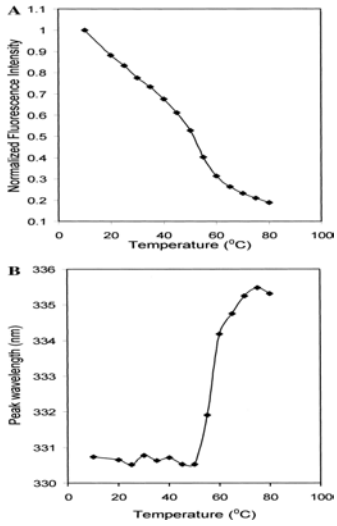

(A) Effect of temperature on rhFVIII fluorescence emission intensity at 330 nm.
(B) Effect of temperature on the fluorescence emission maximum of rhFVIII (B).

Grillo et al. *Biochemistry*, 40 (2), 586 -595, 2001

Effect of temperature on the fluorescence of bis-ANS in the presence of rhFVIII

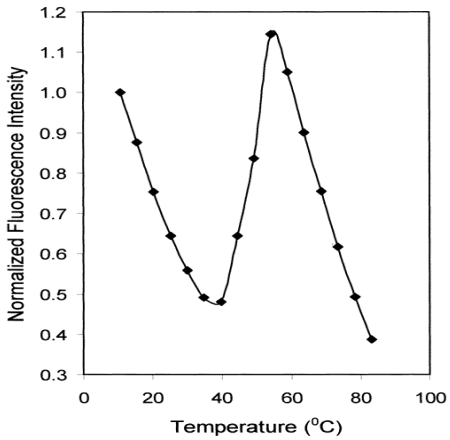

A protein concentration of 0.1 mg/mL and bis-ANS concentration of 4 μM was used in 10 mM MOPS, 150 mM NaCl, 4mM CaCl2, pH 7. Samples were incubated at each temperature for 3 min prior to spectra acquisition. Bis-ANS emission intensity measured at 500 nm.

Grillo et al. *Biochemistry*, 40 (2), 586 -595, 2001

Effect of temperature on the molar ellipticity of rhFVIII at 215 nm

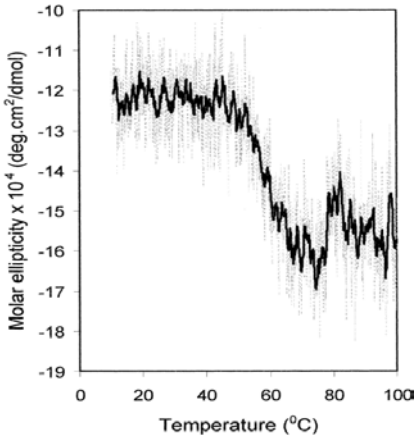

A moving average of the raw data is shown by the dark line for easier visualization of the temperature profile.

Grillo et al. *Biochemistry*, 40 (2), 586 -595, 2001

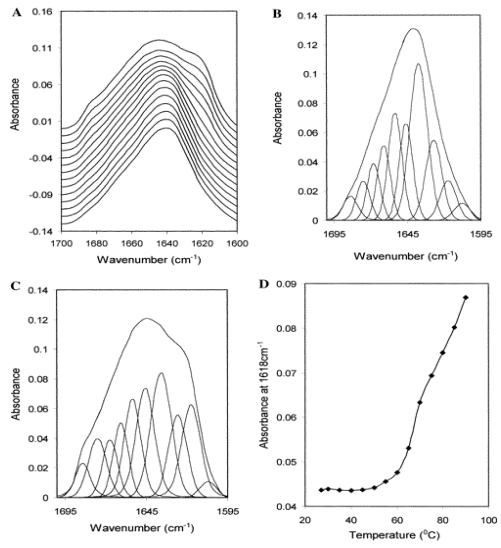

(A)Effect of temperature on the amide I' IR spectrum of rhFVIII. (B) Deconvolution of the amide I' spectrum of rhFVIII obtained at 27 °C. (C) Deconvolution of the amide I' spectrum of rhFVIII at 90 °C. (D) Effect of temperature on the absorbance of rhFVIII at 1618 cm^{-1}.

Grillo et al. *Biochemistry*, 40 (2), 586 -595, 2001

Effect of solute concentration on the wavelength of the fluorescence emission maximum of rhFVIII. GdnHCl is shown in squares, LiClO4 is shown in triangles, urea is shown in diamonds, and propanol is shown in circles

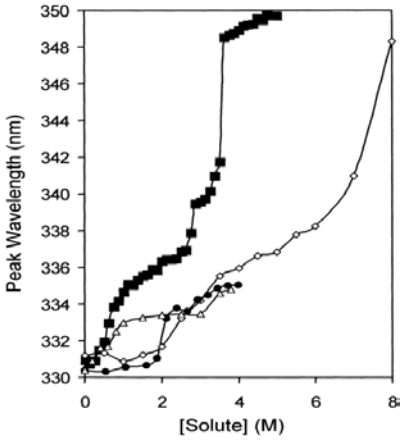

Grillo et al. *Biochemistry*, 40 (2), 586 -595, 2001

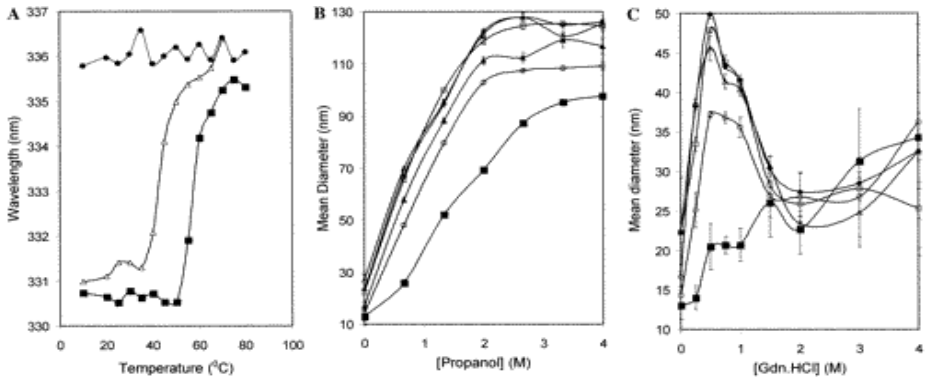

(A) Effect of guanidine hydrochloride concentration on the temperature dependence of the fluorescence emission maximum of rhFVIII: rhFVIII (squares), rhFVIII + 0.5 M GdnHCl (triangles), and rhFVIII + 2 M GdnHCl (circles). (B) Effect of propanol concentration and incubation time (at 37 °C) on rhFVIII size as determined by dynamic light scattering: time 0 (closed squares), day 1 (open circles), day 2 (closed triangles), day 3 (open squares), day 4 (closed diamonds), and day 5 (open triangles). (C) Effect of GdnHCl concentration and incubation time (at 37 °C) on rhFVIII size as determined by DLS: day 0 (closed squares), day 1 (open circles), day 2 (closed triangles), day 3 (open squares), day 4 (closed diamonds).

Grillo et al. *Biochemistry*, 40 (2), 586 -595, 2001

Effect of temperature on the fluorescence wavelength emission maximum of rhFVIII in the absence (squares) and presence (circles) of 40 mM EGTA

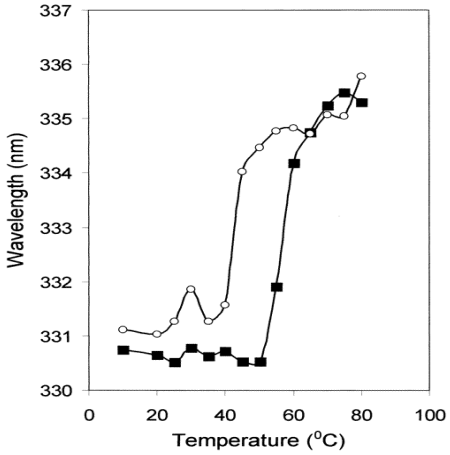

Grillo et al. *Biochemistry*, 40 (2), 586 -595, 2001

The Analysis and Stability of Proteins at High Concentration

The very crowded environment of the cell

Actin (red)

macromolecules, primarily ribosomes (green)

membranes (blue) are represented.

Figure from : Medalia, O., Weber, I., Frangakis, A. S., Nicastro, D., Günther Gerisch, G. and Baumeister, W. *Science* (2002) **298**, 1209-1213.

Background

- Crowded nature of cellular systems
  - Protein concentrations approaching 40% w/v
- Highly concentrated protein formulations
  - Expense of hospitalization[1]
  - Frequent dosing requirements[1]
- Analytical methodologies
  - Molecular modeling/computational analysis[2]
  - Dilute and extrapolate

[1] Lobo, 2004 *J. Pharm. Sci.*

[2] Minton, 2005 *J. Pharm. Sci.*

Excluded Volume Theory

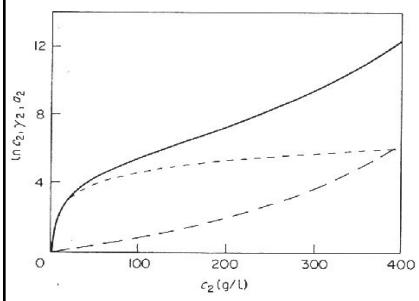

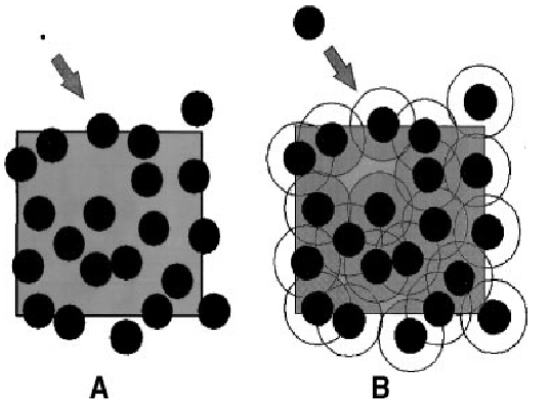

- Ross and Minton, 1977, *Analytical Biochemistry*
- Minton, 2005 *J. Pharm Sci.*

Excluded Volume Theory cont'd.

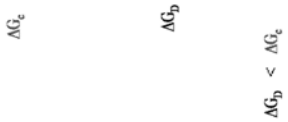

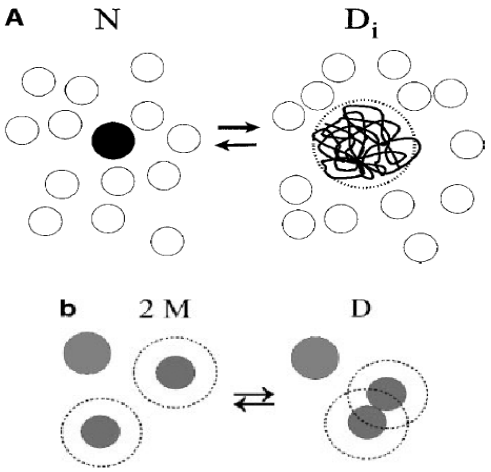

A – Conformational stabilization

b – Colloidal destabilization

- Minton, 2005 *J. Pharm Sci.*

Potential Biophysical Methods to Examine Ultra-high Protein Concentration Formulations

- Tertiary Structure:
  - Front surface fluorescence
  - Ultra-high resolution near ultra-violet absorbance spectroscopy
  - Near-UV circular dichroism spectroscopy
  - Raman spectroscopy
- Secondary Structure:
  - Far-UV circular dichroism spectroscopy
  - FTIR/Raman spectroscopy
- Thermal/Dynamic:
  - Differential scanning calorimetry
  - Pressure perturbation calorimetry
  - Ultra-sonic spectrometry
  - Dynamic light scattering
  - NMR

Specific Aims

- Develop methods to directly study high concentration protein solutions
- Determine the effect of concentration on structure and stability
  - Model Proteins
    - bovine serum albumin 399 mg/mL
    - fibrinogen 50 mg/mL
    - lysozyme 350 mg/mL
    - hemoglobin 245 mg/mL
    - two monoclonal antibodies up to 200mg/mL
    - bovine somatotropin in an oil suspension up to 400mg/mL
  - Methods

DSC	FTIR
UV	CD
FSF	DLS
Raman	US

- What happens to proteins in highly concentrated environments?
  - Conformational Stability
  - Colloidal Stability

DSC

DSC – Model Proteins

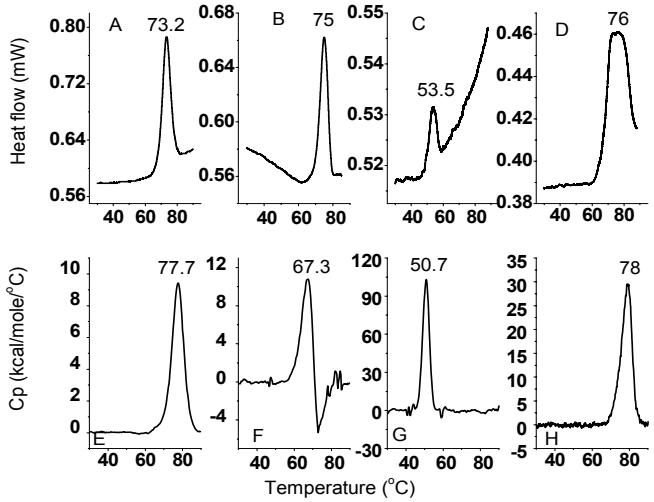

- Lysozyme
  - A. 0.4mg/ml
  - E. 350mg/ml
- Hemoglobin
  - B. 0.3mg/ml
  - F. 245mg/ml
- Fibrinogen
  - C. 0.2mg/ml
  - G. 59mg/ml
- BSA
  - D. 0.6mg/ml
  - H. 399mg/ml

DSC – Monoclonal Antibodies

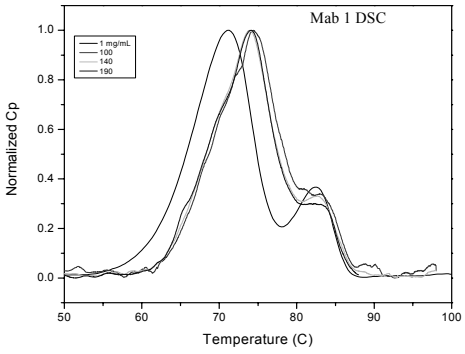

- (—) 1 mg/mL
- (—) 100 mg/mL
- (—) 140 mg/mL
- (—) 190 mg/mL

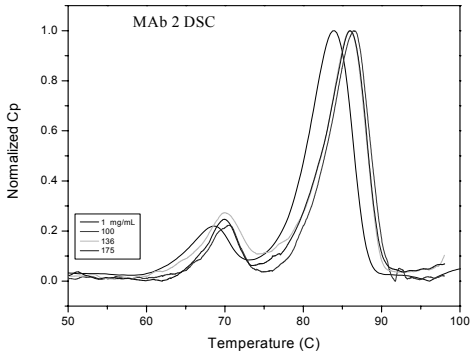

- (—) 1 mg/mL
- (—) 100 mg/mL
- (—) 136 mg/mL
- (—) 176 mg/mL

DSC Summary

- Decreased stability
  - Lysozyme
  - BSA
- Increased stability
  - Hemoglobin
  - Fibrinogen
  - MAb 1
  - MAb 2

Circular Dichroism

- Secondary structure analysis
- Sampling requirements
  - 1-10 µL sample size
  - <10 µm path length
- Spectral artifacts?

CD Spectral Artifact

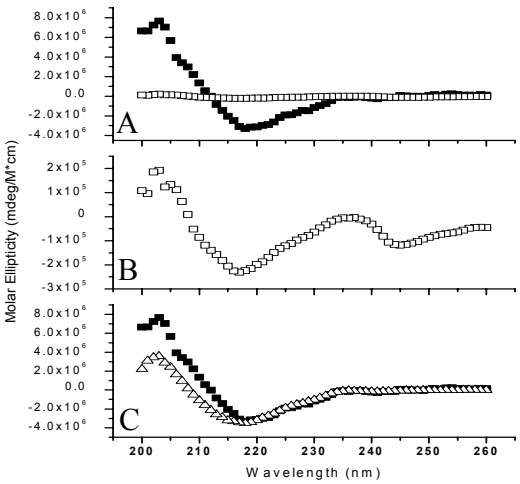

- A. Representative IgG spectra
  - ■ 0.1mg/mL
  - □ 100mg/mL with excessively long path length
- B. A blown up representation of the 100mg/mL spectrum
- C. Representative spectra with effective path length reduction

Far UV CD – Model Proteins

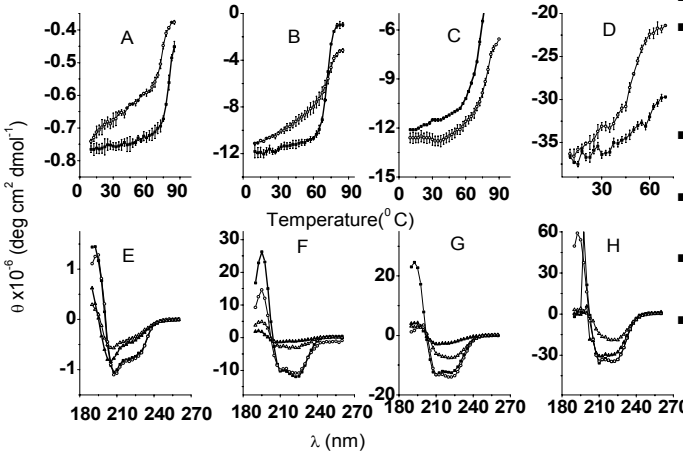

- A-D. Ellipticity at 222nm
- E-H. Far UV CD spectra of proteins at 10°C and at 65°C or 85°C (the end of the melt)
- A/E. Lysozyme
  - ■ 0.4mg/ml; ○ 350mg/ml
- B/F. Hemoglobin
  - ■ 0.3mg/ml; ○ 245mg/ml
- C/G. BSA
  - ■ 0.6mg/ml; ○ 399mg/ml
- D/H. Fibrinogen
  - ■ 0.2mg/ml; ○ 59mg/ml

Far UV CD – Monoclonal Antibodies

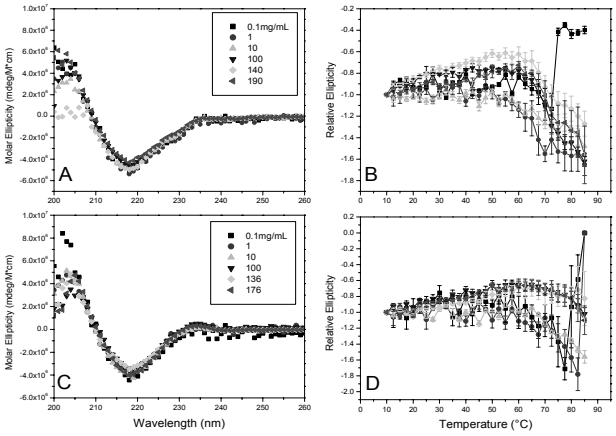

- **A-B. MAb 1**
- (—) 0.1 mg/mL
- (—) 1 mg/mL
- (—) 10 mg/mL
- (—) 100 mg/mL
- (—) 140 mg/mL
- (—) 190 mg/mL
- **C-D. MAb 2**
- (—) 0.1 mg/mL
- (—) 1 mg/mL
- (—) 10 mg/mL
- (—) 100 mg/mL
- (—) 136mg/mL
- (—) 176 mg/mL

CD Summary

- Structural analysis
  - Similar/same spectral signatures initially for all proteins at high and low concentration
- Decreased stability
  - Lysozyme
- No Change
  - Hemoglobin
  - MAb 1
- Increased stability
  - BSA
  - Fibrinogen
  - MAb2

ATR-FTIR

- Attenuated total reflectance FTIR
- Infrared light is reflected through a crystal
- At some points, this light penetrates into sample and is absorbed, creating a small effective path length.

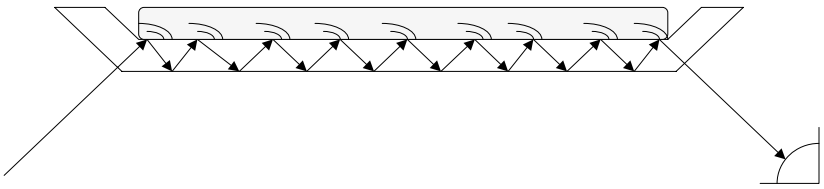

ATR-FTIR – Model Proteins

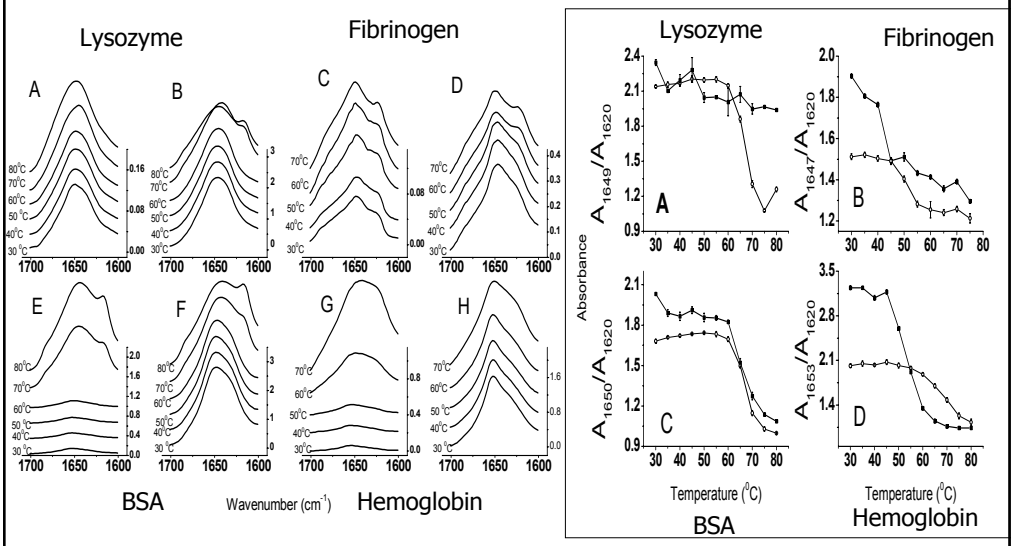

ATR-FTIR – Model Proteins

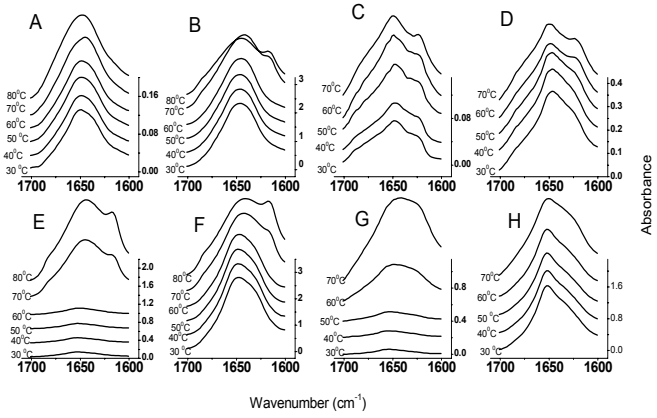

- **Lysozyme**
- A. 10 mg/ml
- B. 400 mg/ml
- **Fibrinogen**
- C. 11mg/ml
- D. 59 mg/ml
- **BSA**
- E. 10 mg/ml
- F. 400 mg/ml
- **Hemoglobin**
- G. 8 mg/ml
- H. 245 mg/ml

ATR/Transmission FTIR

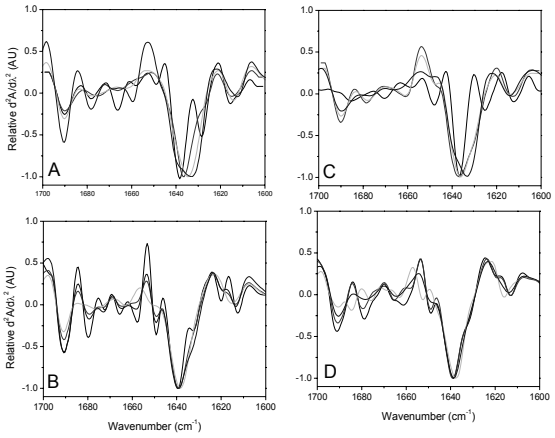

- A. ATR spectra of MAb 1
  - (—) 10mg/mL
  - (—) 100mg/mL
  - (—) 140mg/mL
  - (—) 190mg/mL
- B. Transmission spectra of the same solutions of MAb 1
- C. ATR spectra of MAb 2
  - (—) 10mg/mL
  - (—) 100mg/mL
  - (—) 140mg/mL
  - (—) 180mg/mL
- D. Transmission spectra of the same solutions of MAb 2

FTIR Summary

- Adsorbed protein in ATR?
- Decreased stability
  - Lysozyme
- No Change
  - BSA
  - Fibrinogen
- Increased stability
  - Hemoglobin

Front Surface Fluorescence

Front Surface Fluorescence – Model Proteins

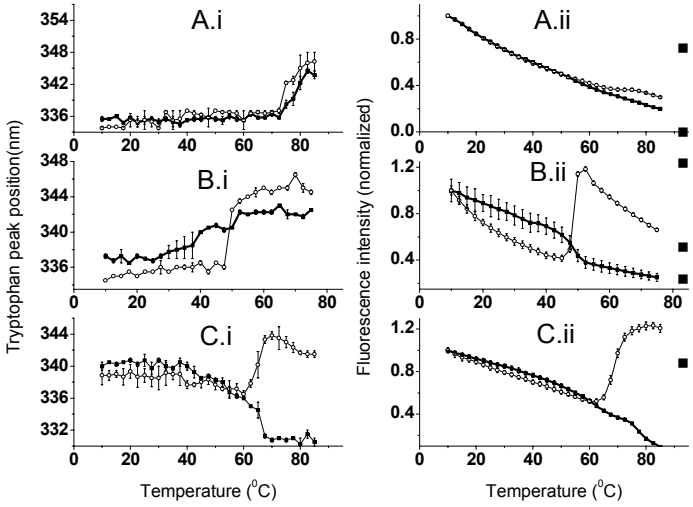

- A.i. λmax **Lysozyme** ■ 0.41mg/ml; ○ 350mg/ml
- A.ii. Intensity at 335nm
- B.i. λmax **Fibrinogen** ■ 0.17mg/ml; ○ 59mg/ml
- B.ii. Intensity at 336nm
- C.i. λmax **BSA** ■ 0.55mg/ml; ○ 399mg/ml
- C.ii. Intensity at 339nm

Front Surface Fluorescence – MAb 1

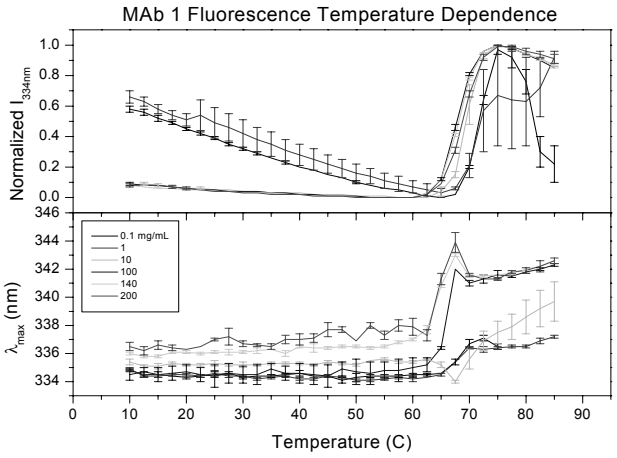

- (—) 0.1 mg/mL
- (—) 1 mg/mL
- (—) 10 mg/mL
- (—) 100 mg/mL
- (—) 140 mg/mL
- (—) 190 mg/mL

Front Surface Fluorescence – MAb 2

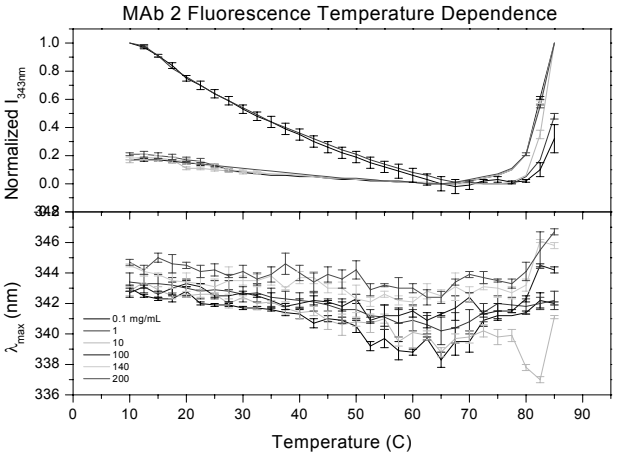

- (—) 0.1 mg/mL
- (—) 1 mg/mL
- (—) 10 mg/mL
- (—) 100 mg/mL
- (—) 136mg/mL
- (—) 176 mg/mL

Front Surface Fluorescence Summary

- Initially similar structure for all proteins at high and low concentration
- Decreased stability
  - Lysozyme
  - MAb 1
  - MAb 2
- No Change
  - BSA
  - Fibrinogen
- No Hemoglobin fluorescence
  - Inner filter effects

High Resolution 2nd Derivative UV Absorbance

- Absorbance requirements
  - 1-10 μm path length
  - <1.5 AU
- OD_{350nm}
- 2nd derivative peak positions of aromatics

2nd Derivative UV Absorbance - Hemoglobin

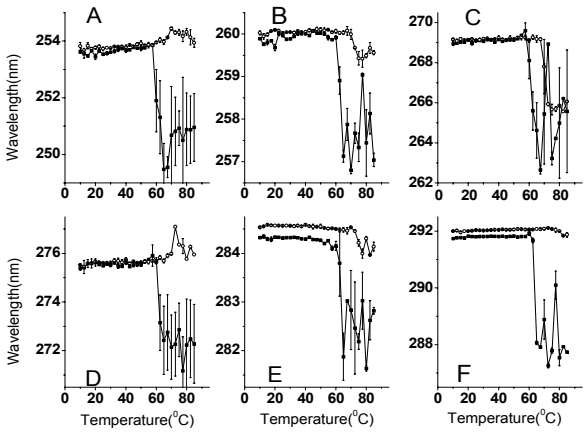

- ■ 0.3mg/ml
- ○ 245mg/ml
- A. Phe
- B. Phe
- C. Phe
- D. Tyr
- E. Tyr/Trp
- F. Trp

2nd Derivative UV Absorbance - Lysozyme

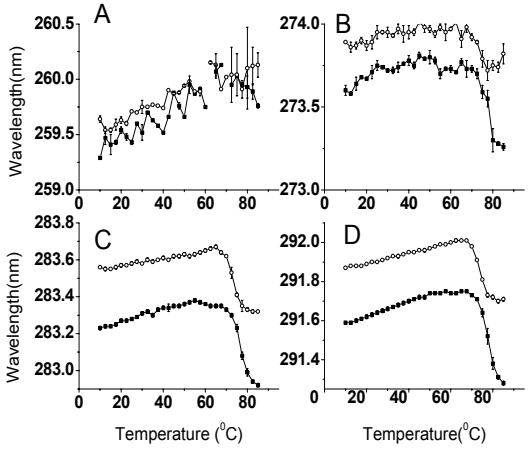

- ■ 0.41mg/ml
- ○ 350mg/ml
- A. Phe
- B. Tyr
- C. Tyr/Trp
- D. Trp

2nd Derivative UV Absorance – Fibrinogen

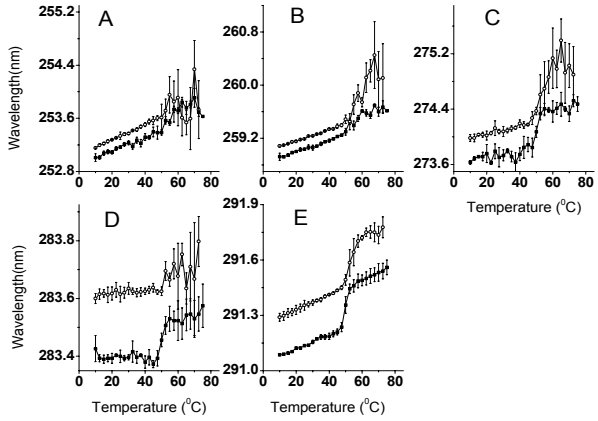

- ■ 0.17 mg/ml
- ○ 59 mg/ml
- A. Phe
- B. Phe
- C. Tyr
- D. Tyr/Trp
- E. Trp

2nd Derivative UV Absorbance – Bovine Serum Albumin

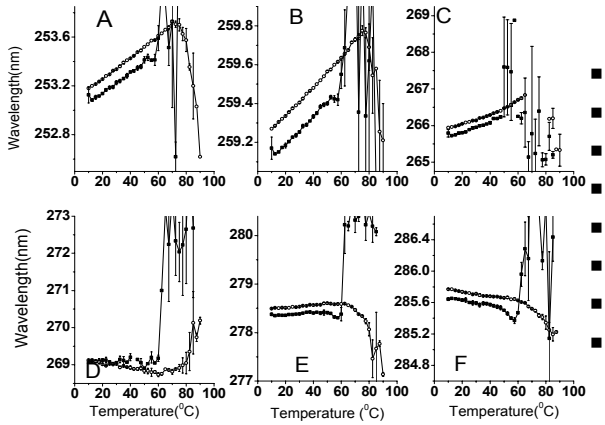

- ■ 0.55 mg/ml
- ○ 399 mg/ml
- A. Phe
- B. Phe
- C. Phe
- D. Tyr
- E. Tyr/Trp
- F. Trp

2nd Derivative UV Absorbance – MAb 1

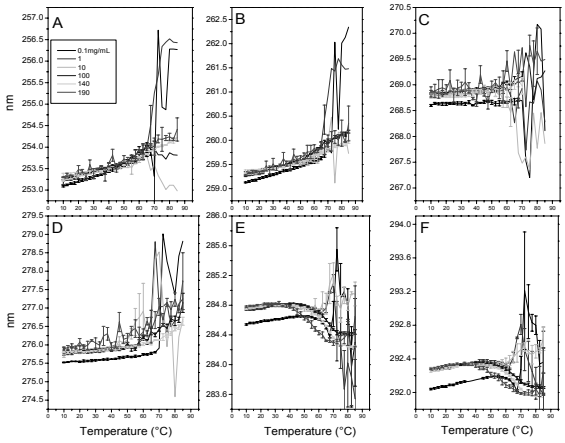

- (—) 0.1 mg/mL
- (—) 1 mg/mL
- (—) 10 mg/mL
- (—) 100 mg/mL
- (—) 140 mg/mL
- (—) 190 mg/mL
- A. Phe
- B. Phe
- C. Phe
- D. Tyr
- E. Tyr/Trp
- F. Trp

2nd Derivative UV Absorbance – MAb 2

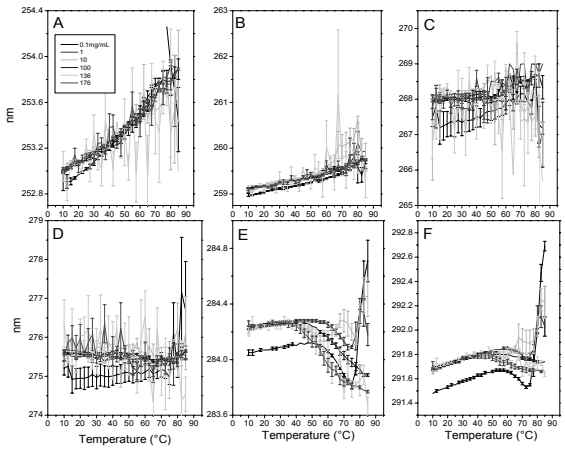

- (—) 0.1 mg/mL
- (—) 1 mg/mL
- (—) 10 mg/mL
- (—) 100 mg/mL
- (—) 136mg/mL
- (—) 176 mg/mL
- A. Phe
- B. Phe
- C. Phe
- D. Tyr
- E. Tyr/Trp
- F. Trp

2nd Derivative Peak Position Summary

- Decreased stability
  - MAb 1
  - MAb 2
- No Change
  - Lysozyme
  - Fibrinogen
  - BSA
- Increased Stability
  - Hemoglobin

Optical Density – Model Proteins

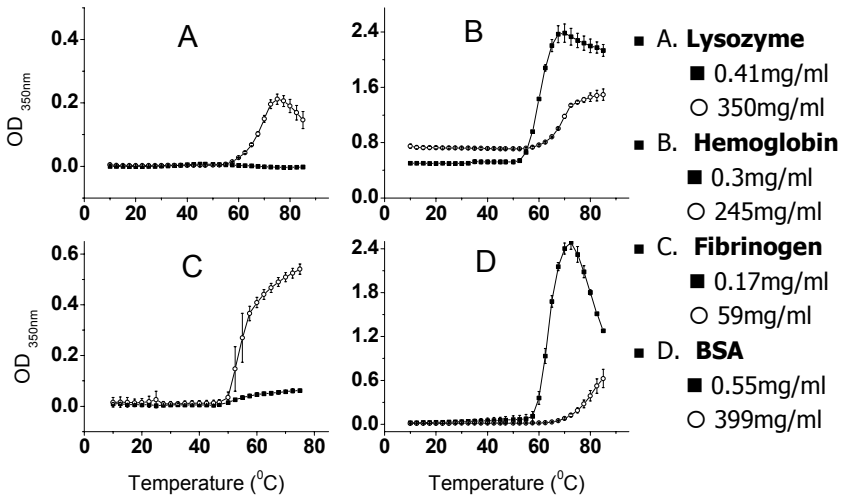

- A. **Lysozyme**
  - ■ 0.41mg/ml
  - ○ 350mg/ml
- B. **Hemoglobin**
  - ■ 0.3mg/ml
  - ○ 245mg/ml
- C. **Fibrinogen**
  - ■ 0.17mg/ml
  - ○ 59mg/ml
- D. **BSA**
  - ■ 0.55mg/ml
  - ○ 399mg/ml

Optical Density - MAbs

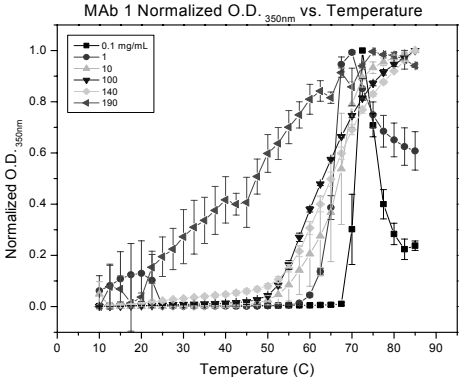

- (—) 0.1 mg/mL MAb 1
- (—) 1 mg/mL
- (—) 10 mg/mL
- (—) 100 mg/mL
- (—) 140 mg/mL
- (—) 190 mg/mL

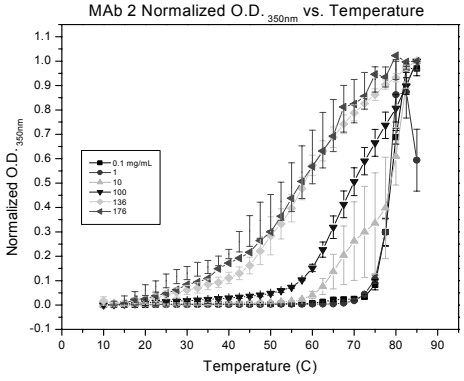

- (—) 0.1 mg/mL MAb 2
- (—) 1 mg/mL
- (—) 10 mg/mL
- (—) 100 mg/mL
- (—) 136mg/mL
- (—) 176 mg/mL

Optical Density – Colloidal Stability Summary

- Decreased stability
  - Lysozyme
  - MAb 1
  - MAb2
- No Change
  - Fibrinogen
- Increased Stability
  - Hemoglobin
  - BSA

Ultra Sonic Spectrometry

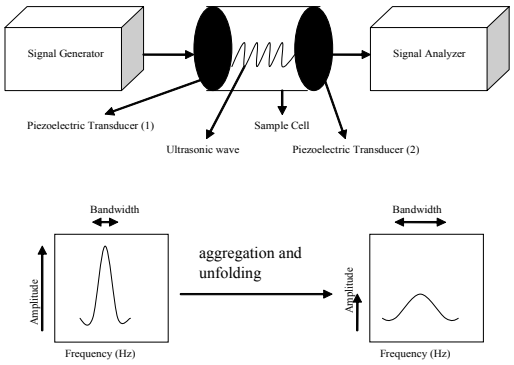

US – 100mg/mL IgG

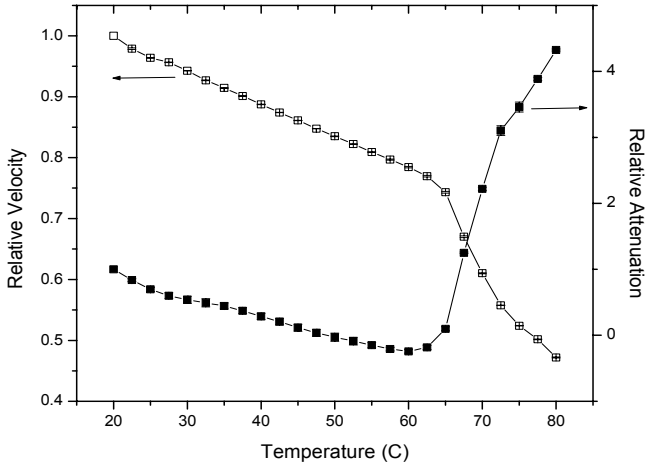

- Although no relative stability obtained yet, potential for compressibility information (dynamic) with this technique.
- Orthogonal method to OD350 for detection of aggregation

Transition Temperatures

Protein	DSC	UV(°C)			O.D.$_{350nm}$	Fluorescence(°C)		CD
(°C)	(°C)	peak4	peak5	peak6	(°C)	λ_{max}	Intensity	(°C)
Lysozyme								
0.41mg/ml	77.7±0.02	75	75	76.7±1.2	No transition	80	No transition	80
350mg/ml	73.2	72.5	73.3±1.2	73.3±1.2	69.3±0.4	75	72.5	74
Hb								
0.3mg/ml	67.0±0.4	62.5	61.3±1.3	63.8±1.3	58.7±0.6	*	*	73±1.5
245mg/ml	75±0.7	64±1	71±2	72±1	68.3±1.2	*	*	73±0.5
Fibrinogen								
0.17mg/ml	50.7±0.2	50±2.0	50	50	53.1±1.1	42.5 ±2.5	47.5	47.5
59mg/ml	53.5±0.1	51.9±2.1	51.7±1.2	52.5±1.8	53.3±1.2	50	47.5	50
BSA								
0.55mg/ml	78±0.2	60[a]	51.3±1.3[a]	50[a]	63.2±0.2	40[a]	46.3±1.3[a]	73.5±1
399mg/ml	76	75[a]	67.5[a]	60[a]	80	60[a]	62.5[a]	78.9±0.5

MAb 1 Empirical Phase Diagram Temp. vs. Concentration (pH 6)

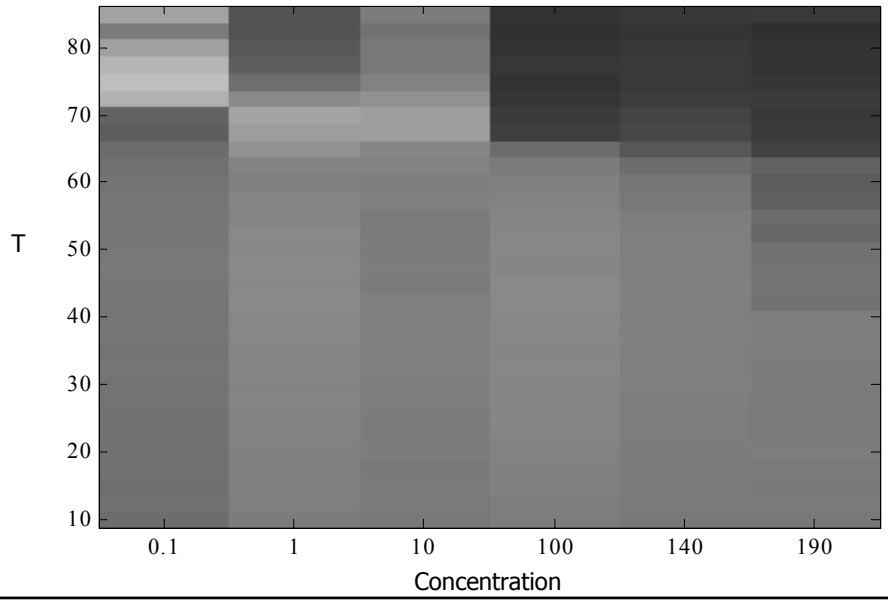

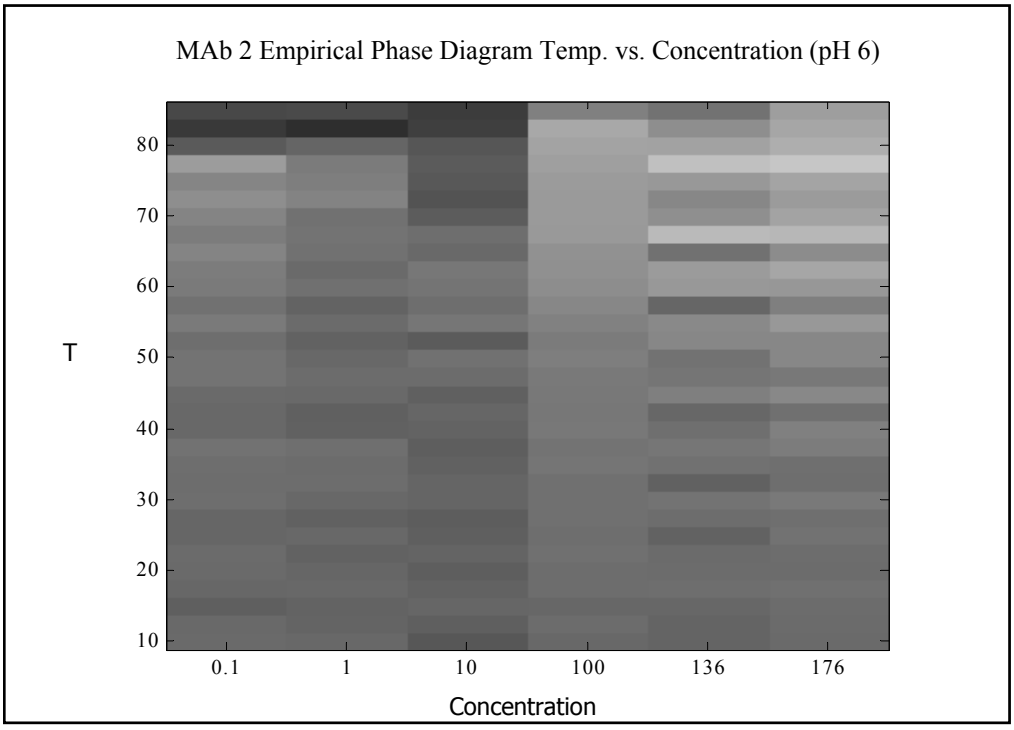

bST in Sesame Oil

bST in Sesame Oil

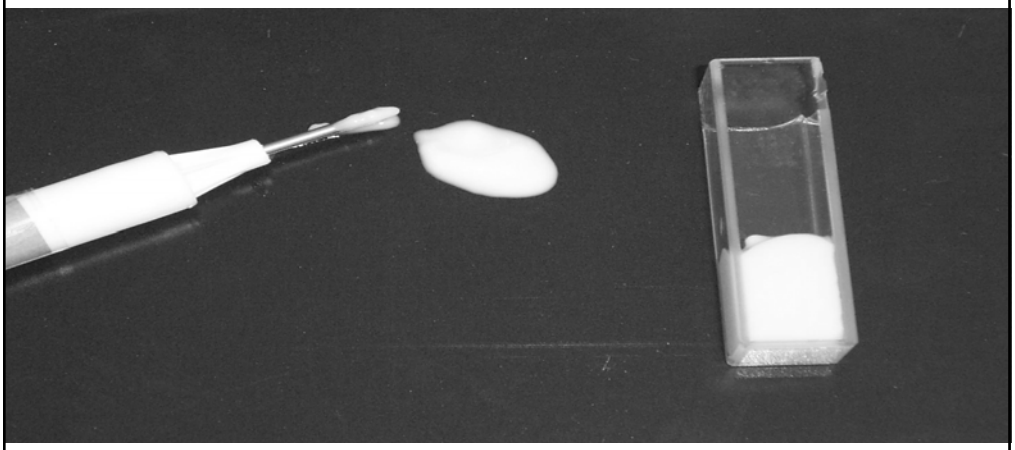

ATR-FTIR - bST

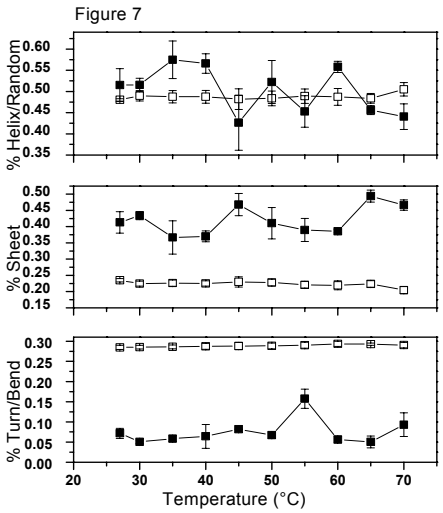

□ Representative oil lot (380mg/mL)

■ 10mg/mL bST in pH 9.5 sodium bicarbonate solution

- Increased stability of oil lot over aqueous solution
- Similar helical/random content in oil and aqueous environments
- Altered sheet and turn contents in oil

Front Surface Fluorescence - bST

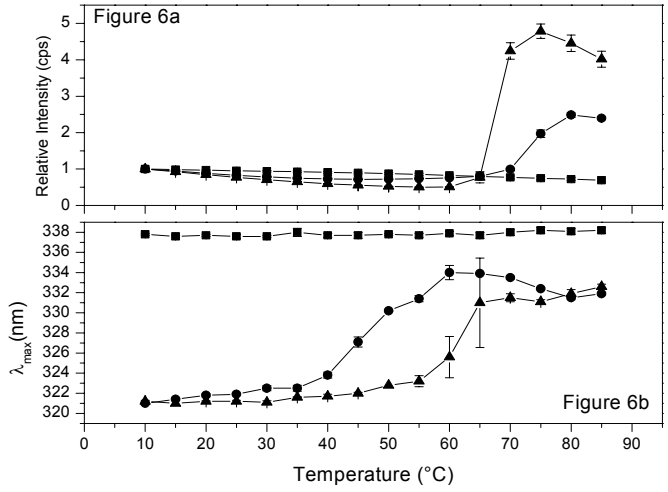

■ Representative oil lot (380mg/mL)

● 10mg/mL bST in pH 9.5 sodium bicarbonate solution

▲ 1mg/mL bST in pH 9.5 sodium bicarbonate solution

• Differences in peak position may reflect the different nature of the samples and not a real structural change

•Oil formulations are more stable than aqueous solutions

• 10mg/mL bST solution is less stable than 1mg/mL bST solution

Front Surface Fluorescence – bST

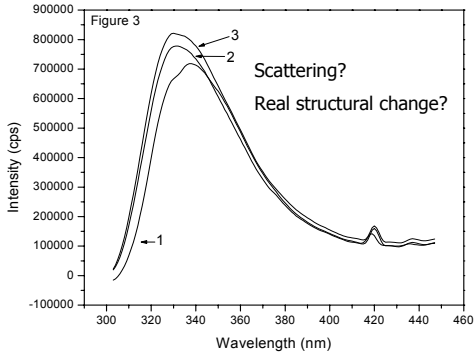

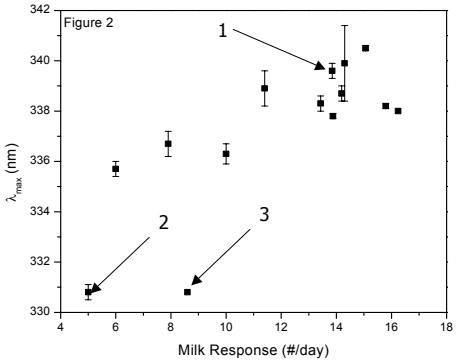

1 – Representative oil spectra of high milk producing lot

2-3 – Representative oil spectra of lower milk producing lots

Aggregate *vs.* Deamidation

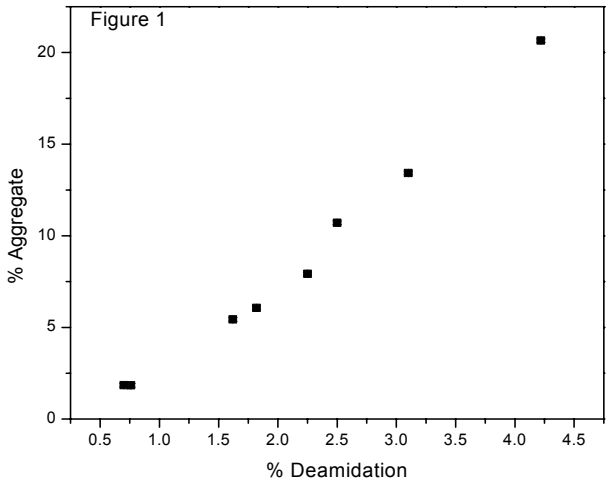

Aim: Measure the fluorescence properties of samples containing increasing aggregate content to elucidate the cause of the altered spectral signatures

Front Surface Fluorescence - bST

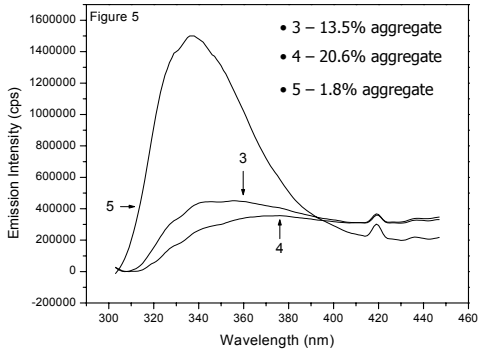

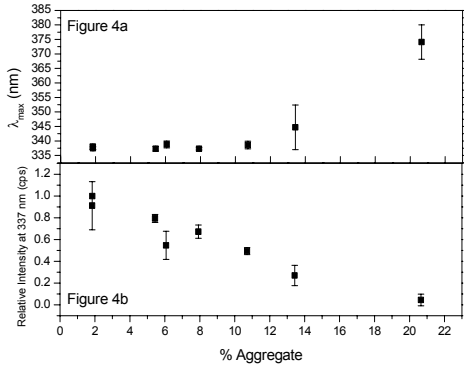

- Severe spectral distortion of high aggregated samples
- Previous spectral changes not due to increased scattering
- Spectral changes likely due to structural perturbation

- Assay demonstrates correlation between fluorescence spectral signals (peak and intensity) with increasing aggregate
- Potential orthogonal method to HP-SEC for measuring aggregate content

Conclusions

- Conformational Stability
  - Secondary Structure – largely stabilized (ex. lysozyme)
  - Tertiary Structure – Variable (decrease – Mabs; increase – Hb)
- Colloidal Stability
  - Variable (decrease – lysozyme and MAbs; increase – Hb)

The Future

- Identifying other driving forces that dictate the stability of proteins at high concentration (other than thermodynamics)
  - Kinetics - Ea
  - Dynamics – flexibility, mobility
  - Interaction phenomena – colloidal stability/aggregation

Acknowledgments

- Nick Harn
- Jianxin Guo
- Medimmune (Chris Allen)
- Monsanto (Yunhua Jeng and Jim Kostele)